






# Hop stunt viroid infection induces heterochromatin reorganization

Joan Marquez-Molins<sup>1,2\*</sup> , Jinping Cheng<sup>1\*</sup> , Julia Corell-Sierra<sup>2</sup> , Vasti Tamara Juarez-Gonzalez<sup>1</sup> , Pascual Villalba-Bermell<sup>2</sup> , Maria Luz Annacondia<sup>1,3</sup> , Gustavo Gomez<sup>2</sup>  and German Martinez<sup>1</sup> 

<sup>1</sup>Department of Plant Biology, Uppsala BioCenter, Swedish University of Agricultural Sciences and Linnean Center for Plant Biology, Uppsala, 75007, Sweden; <sup>2</sup>Institute for Integrative Systems Biology (I2SysBio), Consejo Superior de Investigaciones Científicas (CSIC), University of Valencia (UV), Paterna, 46980, Spain; <sup>3</sup>Department of Plant and Environmental Sciences, Copenhagen Plant Science Centre, University of Copenhagen, Frederiksberg, 1871, Denmark

## Summary

Author for correspondence:  
German Martinez  
Email: [german.martinez.arias@slu.se](mailto:german.martinez.arias@slu.se)

Received: 2 March 2024  
Accepted: 26 June 2024

*New Phytologist* (2024) **243**: 2351–2367  
doi: 10.1111/nph.19986

**Key words:** biotic stress, defense, epigenetics, heterochromatin, histone marks, hop stunt viroid, repressive epigenetic marks, viroids.

- Viroids are pathogenic noncoding RNAs that completely rely on their host molecular machinery to accomplish their life cycle. Several interactions between viroids and their host molecular machinery have been identified, including interference with epigenetic mechanisms such as DNA methylation. Despite this, whether viroids influence changes in other epigenetic marks such as histone modifications remained unknown. Epigenetic regulation is particularly important during pathogenesis processes because it might be a key regulator of the dynamism of the defense response.
- Here we have analyzed the changes taking place in *Cucumis sativus* (cucumber) facultative and constitutive heterochromatin during hop stunt viroid (HSVd) infection using chromatin immunoprecipitation (ChIP) of the two main heterochromatic marks: H3K9me2 and H3K27me3.
- We find that HSVd infection is associated with changes in both H3K27me3 and H3K9me2, with a tendency to decrease the levels of repressive epigenetic marks through infection progression. These epigenetic changes are connected to the transcriptional regulation of their expected targets, genes, and transposable elements. Indeed, several genes related to the defense response are targets of both epigenetic marks.
- Our results highlight another host regulatory mechanism affected by viroid infection, providing further information about the complexity of the multiple layers of interactions between pathogens/viroids and hosts/plants.

## Introduction

Viroids are fascinating biological entities characterized by their extremely simple genomes, short (between 200 and 400-nt) circular noncoding RNAs, that are only pathogenic to plants (Flores *et al.*, 2005; Navarro *et al.*, 2021). Classified as sub-viral pathogens, viroids can be subdivided into two families according to their ability to replicate in the nucleus (*Pospiviroidae*) or the chloroplast (*Avsunviroidae*) (Di Serio *et al.*, 2018, 2021). Due to their remarkably simple genomic organization, viroids must interact with the molecular machinery of the plant cell to fulfill every aspect of their life cycle. As a consequence of this extremely close interaction with their host, viroids induce developmental defects that are identified as symptomatology and are very similar to symptoms caused by viruses (Flores *et al.*, 2005; Navarro *et al.*, 2021). In general, symptom expression is the manifestation of the alteration in the development/defense tradeoff, which, when disturbed, is detrimental to plant growth (Huot *et al.*, 2014). Due to the importance of

maintaining such balance, the defense response is controlled by multiple overlapping mechanisms. Several pieces of evidence indicate that epigenetic pathways are one of the key regulators of stress-associated transcriptional reprogramming (Lamke & Baurle, 2017; Annacondia *et al.*, 2018; Ueda & Seki, 2020). The dynamic nature of the changes introduced by these mechanisms and their known role in the interpretation of environmental and developmental cues in the cellular program makes them good candidates as master regulators of the response to stress (Lamke & Baurle, 2017; Annacondia *et al.*, 2018; Ueda & Seki, 2020). Epigenetic mechanisms comprise both DNA methylation and histone modifications, both of which play a role in the orchestration of genome stability and transcriptional programs (Law & Jacobsen, 2010).

DNA methylation is the best-understood epigenetic mark. It is mediated by the covalent modification of the residue cytosine (C) of the genomic DNA with the addition of a methyl group (Law & Jacobsen, 2010). DNA methylation actively targets transposable elements (TEs, where it accumulates in three sequence contexts: CG, CHG, and CHH, being H any nucleotide other than

\*These authors contributed equally to this work.

C), being also able to target genes similarly to TEs (accumulating in three sequence contexts) or exclusively marking the gene body (accumulating only in the CG context) (Tran *et al.*, 2005; Law & Jacobsen, 2010). This targeting induces the silencing of both TEs and genes (Muyle *et al.*, 2022). In addition to DNA methylation, plants have another conserved epigenetic mechanism consisting of posttranslational modifications of the histone tails that are part of the nucleosome (Malik & Henikoff, 2003). These modifications define the interactions between neighboring nucleosomes, leading to the formation of two different levels of chromatin compaction: euchromatin and heterochromatin, that contain loosely or highly compacted nucleosomes, the latest being recalcitrant to RNA polymerase II-mediated transcription (Becker *et al.*, 2017). Heterochromatin can be further divided into two different structural forms: facultative and constitutive, which are dynamic or not to developmental/environmental signals (Becker *et al.*, 2017; Hu *et al.*, 2019). Interestingly, both forms of heterochromatin have different genomic targets and deposition machinery.

Facultative heterochromatin is marked by the trimethylation of the lysine 27 of histone 3 (H3K27me<sub>3</sub>), which is located in gene-rich genomic regions within the arms of the chromosomes (Liu *et al.*, 2010; Feng & Michaels, 2015). H3K27me<sub>3</sub> is controlled by the protein complexes Polycomb repressive complex 1 and 2 (PRC1 and PRC2) and marks the promoters and transcriptional start sites of specific genes (Ng *et al.*, 2007; Zhang *et al.*, 2007; Schuettengruber *et al.*, 2011; Mozgova *et al.*, 2015). Recent pieces of evidence indicate that, additionally, H3K27me<sub>3</sub> controls the formation of repressive chromatin hubs (Huang *et al.*, 2021). H3K27me<sub>3</sub> is a key regulatory epigenetic mark that controls a myriad of developmental events including flowering time, circadian clock, sensing of temperature, and gene imprinting (He *et al.*, 2012; Gan *et al.*, 2015; Moreno-Romero *et al.*, 2019; Batista & Kohler, 2020; Cheng *et al.*, 2020; Shen *et al.*, 2021; Kim *et al.*, 2023). On the other hand, constitutive heterochromatin is marked by several histone marks, including H3K27me<sub>1</sub>, H3K9me<sub>1</sub>, and H3K9me<sub>2</sub> (Lippman *et al.*, 2004). This type of heterochromatin is enriched in centromeric and pericentromeric regions where it targets TEs and other repetitive sequences. H3K9 methylation is mediated by members of the SUVH class (SU(VAR)3–9 homologs (SUVH) and SU(VAR)3–9 related proteins) (Lippman *et al.*, 2004). In plants, H3K9 methylation is mechanistically connected to DNA methylation, via the ability of SUVH members to recognize non-CG methylation (Ng *et al.*, 2007; Liu *et al.*, 2010; Feng & Michaels, 2015), which creates a feedback loop with the methyltransferase CMT3, which can recognize H3K9 methylation (Matzke & Mosher, 2014). Alternatively, H3K9 methylation can also be established without a premethylated DNA state (Xu & Jiang, 2020).

Both epigenetic mechanisms (DNA methylation and histone marks) have been identified as active players in the response against stress in both genetic (Agorio & Vera, 2007; López *et al.*, 2011; Yu *et al.*, 2013) and genome-wide (Downen *et al.*, 2012; Annacondia *et al.*, 2021, 2023; Dvorak Tomastikova *et al.*, 2021) studies. Particularly, DNA methylation is a dynamic stress-responsive epigenetic

mark under both biotic and abiotic stresses (Pavet *et al.*, 2006; Boyko *et al.*, 2007; Raja *et al.*, 2008; Downen *et al.*, 2012; Gohlke *et al.*, 2013; Yu *et al.*, 2013; Le *et al.*, 2014; Martinez *et al.*, 2014; Castellano *et al.*, 2015, 2016a; Doucet *et al.*, 2016; Hewezi *et al.*, 2017; Wang *et al.*, 2018) that can even be transmitted transgenerationally (Wibowo *et al.*, 2016; Stassen *et al.*, 2018). Histone marks also play a role in the regulation of stress-associated transcriptional reprogramming (Zhou *et al.*, 2005; Wu *et al.*, 2008; Pecinka *et al.*, 2010; Zheng *et al.*, 2012; Choi *et al.*, 2012; Ramirez-Prado *et al.*, 2018; Annacondia *et al.*, 2021; Wang *et al.*, 2021). Different histone marks have been associated with the regulation of the defense response, including both transcription activating marks such as histone acetylation, histone ubiquitination, H3K4 methylation, H3K36me<sub>3</sub>, and the histone variant H2A.Z (Zhou *et al.*, 2005; Alvarez-Venegas *et al.*, 2007; March-Díaz *et al.*, 2008; Wu *et al.*, 2008; Dhawan *et al.*, 2009; Berr *et al.*, 2010; Palma *et al.*, 2010; Jaskiewicz *et al.*, 2011; López *et al.*, 2011; Coleman-Derr & Zilberman, 2012; Choi *et al.*, 2012; Singh *et al.*, 2014; Berriri *et al.*, 2016; Lee *et al.*, 2016; Wang *et al.*, 2017; Li *et al.*, 2020; Sheikh *et al.*, 2023), and transcription repressive marks such as H3K9me<sub>2</sub> and H3K27me<sub>3</sub> (Li *et al.*, 2013; Dutta *et al.*, 2017; Chan & Zimmerli, 2019; He, 2019; Ramirez-Prado *et al.*, 2019; Zeng *et al.*, 2019; Cambiagno *et al.*, 2021; Dvorak Tomastikova *et al.*, 2021; Annacondia *et al.*, 2023). In addition, other factors involved in the stability of the chromatin, such as chromatin remodelers and the linker histone H1 have been connected to the activation of immunity (Yi *et al.*, 2004; Lee *et al.*, 2023; Sheikh *et al.*, 2023). Despite this evidence, the genome-wide dynamism and genomic targets of histone marks have not been studied in detail until recently (Zeng *et al.*, 2019; Dvorak Tomastikova *et al.*, 2021; Annacondia *et al.*, 2023).

Nuclear viroid infection has been reported to induce both the hypomethylation of ribosomal repeats and TEs in several species (Martinez *et al.*, 2014; Castellano *et al.*, 2015, 2016a; Marquez-Molins *et al.*, 2023), and the hypermethylation of host genes (Lv *et al.*, 2016; Marquez-Molins *et al.*, 2023) and co-infective DNA viruses (Torchetti *et al.*, 2016). Whether these changes are connected to histone marks is completely unexplored. Interestingly, viroids can interfere with Histone Deacetylase 6 (HDA6) suggesting a potential effect over the histone mark homeostasis (Castellano *et al.*, 2016b). Despite this evidence, there is a substantial lack of genome-wide studies identifying both the targets and extent of epigenetic changes (especially histone marks) associated with viroid pathogenesis. Here, to understand the dynamism of repressive histone marks during viroid infection, we studied the genome-wide presence of the repressive histone marks H3K9me<sub>2</sub> and H3K27me<sub>3</sub> and their correlation with both DNA methylation and transcription in response to hop stunt viroid (HSVd) infection in cucumber, at two different time points. We found that HSVd leads to a reorganization of H3K9me<sub>2</sub> and H3K27me<sub>3</sub> characterized by a decrease in the presence of both marks over repeats and different patterns of dynamism over genes. Importantly, H3K27me<sub>3</sub> is globally correlated with transcriptional changes, including several stress-responsive genes that might be important to respond to

viroid infection. In summary, our data offers a novel perspective on viroid–host interactions and the interplay between heterochromatin dynamism and the response to adverse environmental conditions in plants.

## Materials and Methods

### Plant material and HSVd infection

*Cucumis sativus* L. (variety Marketer) were sown into potting soil (P-Jord, Hasselfors Garden, Örebro, Sweden) into plastic pots (9 × 9 × 7 cm) with one plant per pot at a temperature of 30°C and 60% relative humidity. Plants were grown under a 16 h : 8 h, light : dark photoperiod. The light was provided by FQ, 80 W, Hoconstant lumix (Osram, Munich, Germany) with a light intensity of 220 μmol photons m<sup>-2</sup> s<sup>-1</sup>. HSVd infection was performed at the two-cotyledon stage. Seedlings were agroinfiltrated with an infectious HSVd clone or an empty vector (mock plants) (Marquez-Molins *et al.*, 2019). Samples were collected at 10 and 27 d postinfection (dpi).

### Chromatin immunoprecipitation (ChIP) sequencing libraries preparation and sequence analysis

First, 500 mg of systemic leaves were chemically cross-linked using 1% formaldehyde. Then, nuclei were isolated from cross-linked material following a standard nuclei isolation protocol based on sucrose gradients as previously described by (Moreno-Romero *et al.*, 2016). The resuspended nuclei pellets were sonicated for 9 cycles of 20 s on and 45 s off at 4°C and high power to obtain the chromatin. Afterward, the immunoprecipitation (IP) was performed following a standard IP protocol and using the following antibodies: H3 (Reference: 07-690; Merck KGaA, Darmstadt, Germany), H3K9me2 (Reference: pAb-060-050; Diagenode, Seraing, Belgium), and H3K27me3 (Reference: 07-449; Merck KGaA). The resulting immunocomplexes were purified with the GeneJET PCR Purification Kit (Thermo Fisher, Bremen, Germany), following the manufacturer's instructions. Finally, DNA libraries were prepared using the NEBNext<sup>®</sup> Ultra<sup>™</sup> II DNA Library Prep Kit for Illumina<sup>®</sup> (New England Biolabs, Frankfurt am Main, Germany) and each library was barcoded using the NEBNext<sup>®</sup> Multiplex Oligos for Illumina<sup>®</sup> kit (New England Biolabs).

ChIP libraries of two bioreplicates per condition were obtained from the immunoprecipitated DNA and sequenced as paired-end 150 bp fragments in an Illumina Novaseq 6000 at Novogene (Beijing, China). The obtained raw reads were trimmed using TRIMGALORE 0.6.1 to remove the adapter sequences and 10 bases from 5' ends. For genome-wide distribution analysis sequences were aligned to the *Cucumis sativus* 'Chinese long' v.3 genome (Li *et al.*, 2019) using BOWTIE2 with default parameters. BAM files were filtered for unique reads using the parameter -q10 and replicates were merged using SAMTOOLS (Li *et al.*, 2009). Genome coverage was calculated as the log<sub>2</sub> fold change of the ratio between the coverage of H3K9me2 or H3K27me3 to the coverage of H3 using DEEPTOOLS2 (Ramirez *et al.*, 2016). For genome-wide profile

images, the RPKM-normalized value of H3 was subtracted from the RPKM value of either H3K9me2 or H3K27me3. Values for specific regions and quantitative analysis were retrieved using MAPBED from BEDTOOLS (Quinlan & Hall, 2010).

For peak identification, reads were aligned to the *Cucumis sativus* 'Chinese long' v.3 genome (Yu *et al.*, 2023) using BOWTIE2, with the options --no-mixed --no-discordant. BAM files were filtered for unique reads and high-quality alignments using the parameters -q 10 and -F 256 using SAMTOOLS. Peak calling was performed using SICER2 for each sample to its respective H3 control with the parameters window size 200, fragment size 150, effective genome fraction 0.74, false discovery rate 0.01, false discovery rate of 0.01, and a gap size of 600 bp. Peak location and overlap were compared using the intersect tool from BEDTOOLS with a minimum overlap of 1 bp. Only peaks shared between the two replicates were considered true peaks for that specific treatment. Shared peaks were compared between samples using the intersect tool from bedtools to determine gain and loss peaks. Sequencing results were validated from the sequencing library cDNAs using quantitative PCR. The relative enrichment of each mark (normalized to H3) was determined using the 2<sup>-ΔΔCt</sup> method with the primers indicated in Supporting Information Table S1.

### Gene ontology (GO) term analysis

GO term analysis was performed using the GO annotation for the *Cucumis sativus* 'Chinese long' v.3 (<http://cucurbitgenomics.org/organism/20>) (Yu *et al.*, 2023). GO categories were simplified to the GO Slim Classification for Plants.

### DNA methylation and RNA sequencing reanalysis

DNA methylation values were obtained from the previous analysis in Marquez-Molins *et al.* (2023). RNA sequencing libraries from the same study (Marquez-Molins *et al.*, 2023) were filtered to infer the expression level of repeats. In brief, the count reads per repeat was obtained using HTSEQ-COUNTS with the following parameters: --mode union --stranded no --minequal 0 and --nonunique all. The obtained count tables were used in DESEQ2 (Love *et al.*, 2014) to infer significant expression with fit type set to parametric. All these tools were used on the Galaxy platform (Afgan *et al.*, 2018). Volcano plots were created using the R package GGPLOT2 (Hadley, 2016).

### Immunolocalization

Immunostaining of *Cucumis sativus* nuclei was performed as previously described (Yelagandula *et al.*, 2014). In brief, 10- and 27-d postinfection (mock and HSVd-infected) leaves were collected and fixed in cold 4% paraformaldehyde in Tris–HCl buffer (10 mM Tris pH 7.5, 10 mM EDTA and 100 mM NaCl) for 20 min followed by two washes with ice-cold Tris–HCl buffer twice for 10 min each. Nuclei were isolated by chopping leaves in LB01 buffer (15 mM Tris–HCl pH 7.5, 20 mM NaCl, 2 mM EDTA, 80 mM KCl, 0.5 mM spermine, 0.1% Triton-X-

100) and filtered through a 30- $\mu\text{m}$  Cell Trics filter (Sysmex, Norderstedt, Germany). The filtered nuclei were diluted 1 : 3 with sorting buffer (100 mM Tris pH 7.5, 50 mM KCl, 2 mM  $\text{MgCl}_2$ , 0.05% Tween 20, 5% sucrose), and spotted onto microscopy slides to air-dry. The slides were postfixed with 4% paraformaldehyde for 15 min at room temperature in PBS buffer (10 mM sodium phosphate, pH 7.0, 143 mM NaCl), and washed twice with PBS for 5 min each. Slides were blocked with 4% BSA for 30 min at 37°C in a moist box followed by primary (anti-H3K9me2, C15410060, Diagenode, 1 : 500; anti-H3K27me3, 07-449, Merck KGaA, 1 : 500) and secondary (Alexa Fluor 488 Goat anti-Rabbit IgG1 Secondary Antibody, A21121, Invitrogen, 1 : 100) antibody incubation (all diluted in 1% BSA, 0.1% tween20, 1 $\times$  PBS). After the antibody incubations, slides were mounted with 2  $\mu\text{g ml}^{-1}$  DAPI and analyzed in a confocal microscope (Zeiss LSM780). Quantification of area and intensity of the fluorescent signal was performed using IMAGEJ (Schneider *et al.*, 2012).

## Results

### Overview of *Cucumis sativus* heterochromatin

Previous studies have shown that alterations in DNA methylation patterns are dynamic under HSVd infection and are an important component of the reprogramming of the defense response against this sub-viral pathogen (Martinez *et al.*, 2014; Castellano *et al.*, 2015, 2016a; Marquez-Molins *et al.*, 2023). The involvement of other epigenetic mechanisms such as histone marks that could respond to viroid infection could be inferred from their direct interaction with HDA6 (Castellano *et al.*, 2016b) but their overall genome-wide changes are not understood. Heterochromatin, composed of facultative and constitutive regions, is an important genomic structure controlling the stability of the genome and the expression of genes. To understand the dynamism and genome-wide changes taking place in heterochromatin under viroid infection, we performed ChIP-sequencing for the two best-studied heterochromatic histone modifications H3K27me3 and H3K9me2 in cucumber plants infected with HSVd at two different time points: 10 d postinfection (dpi, onset of infection) and 27 dpi (development of symptoms) equivalent to the time points used in Marquez-Molins *et al.* (2023) (Fig. S1).

Our ChIP offered a unique opportunity to study heterochromatin in cucumber, which was not yet described. In mock tissues, the distribution of the two histone marks showed a similar pattern to the one observed in other plants such as *Arabidopsis thaliana* (Roudier *et al.*, 2011). H3K9me2 accumulated to a higher level in centromeric regions enriched in repeats, while H3K27me3 was enriched in the arms of the chromosomes where the density of repeats is lower (Fig. 1a). As expected from this pattern, genes are preferentially marked by H3K27me3 (Figs 1b, S2A), while repeats are usually marked by H3K9me2 (Figs 1c, S2B). Targets of both marks included well-studied epigenetically regulated examples such as an FLC homolog in cucumber (CsaV3\_3G016650) targeted by H3K27me3 and a long Gypsy

TE targeted by H3K9me2 (Fig. S3). We further verified this different localization of both marks by employing immunolocalization with specific antibodies (Fig. 1d). Our analysis confirmed the preferential localization of H3K9me2 in heterochromatin since its signal overlapped with DAPI-stained heterochromatic chromocenters and the diffused distribution of H3K27me3 through the nucleus outside of chromocenters (Fig. 1d). The enrichment of H3K9me2 among repeats was more obvious among TEs, with members of the Gypsy, LINE, and Copia retrotransposon superfamilies showing higher values of this repressive mark compared to other DNA transposon superfamilies such as hAT-AC, MuDR and En-SPM (Fig. 1e). Interestingly, we observed a reduction of H3K9me2 at 27 d, which might be connected to the senescence of the plants, as previously observed in dark-induced senescent tissues of *A. thaliana* (Trejo-Arellano *et al.*, 2020). TEs that presented high values of H3K9me2 had characteristics of heterochromatic entities, such as longer length and closer distance to the centromere (Fig. S4A,B). As expected, longer TEs tend to have higher values of H3K9me2 (Fig. S4C), a characteristic that is not present for H3K27me3 and genes (Fig. S4D).

Next, to understand their enrichment at specific locations in the cucumber genome we analyzed the presence of histone peaks (bioinformatically identified regions enriched for each of our studied marks compared to our H3 control, see material and methods for the parameters used for defining peaks) for both marks at the two time points studied. Identification of peaks for the two marks showed that, on average, they occupied 10% of the cucumber genome (Fig. 1f), similar to the inferred percentages from the cytogenetic mapping (Sun *et al.*, 2013). As expected from the different compartmentalization of the marks in genes and repeats (Fig. 1b,c), peaks for the two marks showed little to no overlap (Fig. 1g), indicating that they virtually mark two different genomic regions, as confirmed by our immunolocalization analysis (Fig. 1d). A characteristic of plant DNA methylation is that overall low DNA methylation levels increase at centromeric and pericentromeric regions (Cokus *et al.*, 2008), where it targets TEs and other repeats (Law & Jacobsen, 2010). Similar to most plant species, there is a significant presence of DNA methylation at H3K9me2 peaks that does not happen at H3K27me3 peaks, suggesting that the RdDM pathway might be directly involved in the establishment of H3K9me2 in cucumber and that DNA methylation represses H3K27me3 (Fig. 1h). To further explore the lack of correlation between DNA methylation and H3K27me3, we analyzed the distribution of this mark over genes with different levels of DNA methylation, classified as CG-methylated (CG values > 10% and non-CG values < 10%), TE-like genes (non-CG values > 10%), and unmethylated genes (< 10% methylation in any context). As expected (Liu *et al.*, 2021), unmethylated genes showed the highest enrichment on H3K27me3, while CG-methylated genes showed a moderate, but significant, increase on this mark compared to genes with TE-like methylation (Fig. S4E). In summary, cucumber presented several conserved traits in its heterochromatin, including the characteristic targeting of TEs by H3K9me2 and genes by H3K27me3 observed in other plant species.

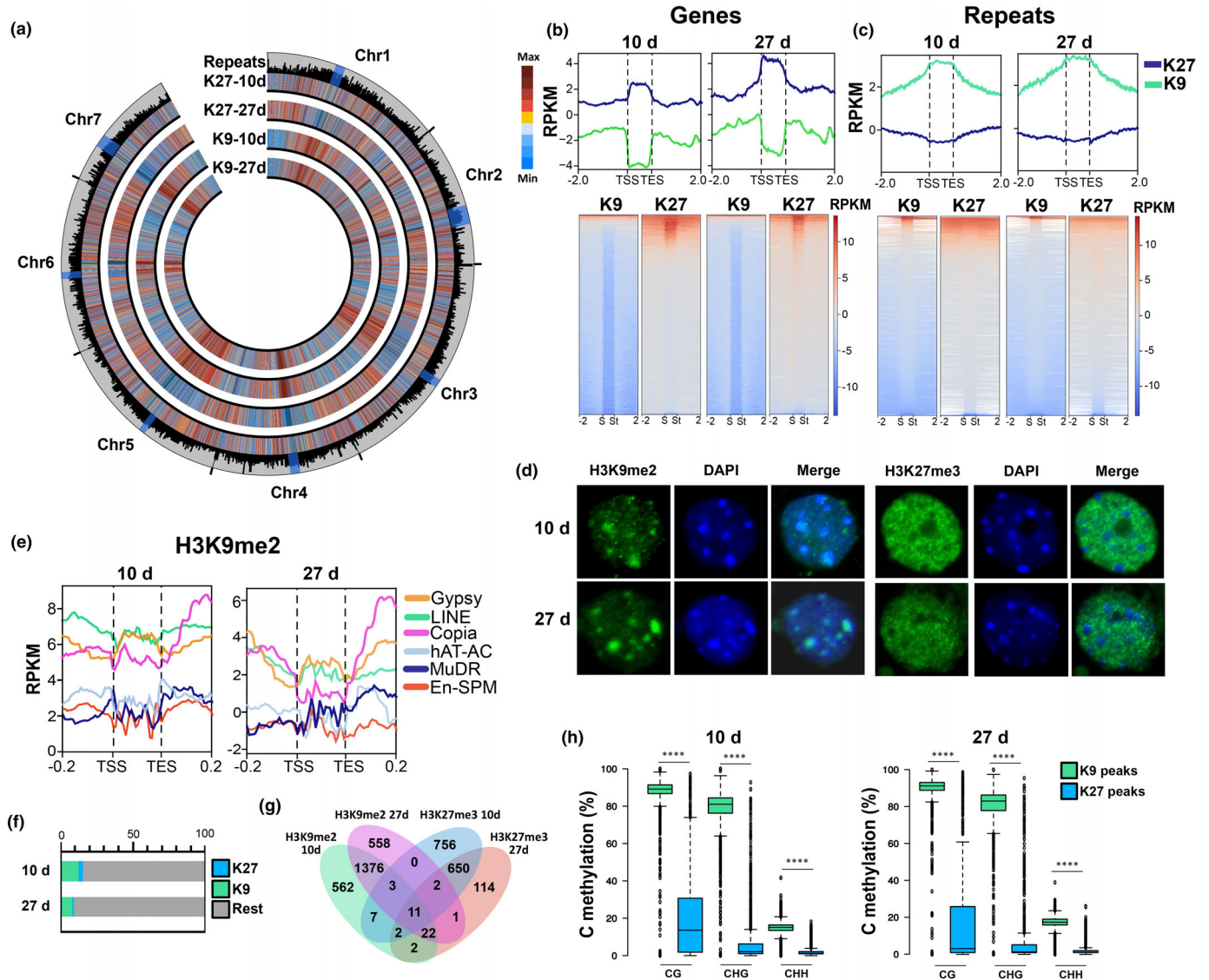


**Fig. 1** An overview of *Cucumis sativus* heterochromatin. (a) Circular plot showing the genome-wide levels of H3K27me3 (K27) and H3K9me2 (K9) in mock samples at 10 and 27 dpi (10 d and 27 d). The outermost track indicates the location and length of the repeats present in the *C. sativus* genome. The location of centromeres according to the cytogenetic analysis from Sun *et al.* (2013) is shown in blue. (b, c) Histone modification coverage profiles for genes (b) and repeats (c) in mock samples at 10 and 27 dpi. Graphs represent a 2 kb window (lower units) from the transcriptional start site (TSS) and the transcriptional end site (TES). Heatmaps of the values used for the profile graphs are also shown with the transcriptional start site indicated as 'S' and the transcriptional end site indicated as 'St'. (d) Representative images of H3K9me2 and H3K27me3 immunostained nuclei from cucumber leaves. DAPI-stained chromocenters are shown as a reference of constitutive heterochromatin location. Merge of the GFP and DAPI channels is shown to indicate the overlap of both signals. (e) Histone modification coverage profiles for different TE superfamilies in mock samples at 10 and 27 dpi. Only TEs longer than 2 kb were considered for the representation. Graphs represent a 0.2 kb window (lower units) from the transcriptional start site (TSS) and the transcriptional end site (TES). (f) Percentage of the genome-wide coverage for the peaks identified for each of the histone marks analyzed. (g) Venn diagram showing the overlapping between the peaks identified in mock tissues for each of the histone marks at 10 and 27 d (10 d and 27 d). (h) Values of cytosine methylation percentage for each methylation context for peaks identified on each of the histone marks analyzed. K27 = H3K27me3; K9 = H3K9me2. \*\*\*\* indicates a *P*-value smaller than 0.001. *P*-values were calculated through an unpaired *t*-test. Boxplots are Tukey's style (whiskers extend to data points that are  $< 1.5 \times$  IQR away from the 1<sup>st</sup>/3<sup>rd</sup> quartile).

### H3K9me2 and H3K27me3 are reorganized during the progression of HSVd infection

To understand the dynamism experienced by both heterochromatic marks during HSVd infection, we focused on exploring the changes occurring in infected tissues at the two time points under study.

First, regarding H3K9me2, at the genome-wide level, HSVd infection did not induce dramatic changes in the distribution of H3K9me2 at any of the two infection points (Fig. 2a). Indeed, H3K9me2 changes were only significant at later infection times, where it was gained at genes (Fig. 2b) and lost from repeats (Fig. 2c). The striking difference in the presence of this mark at

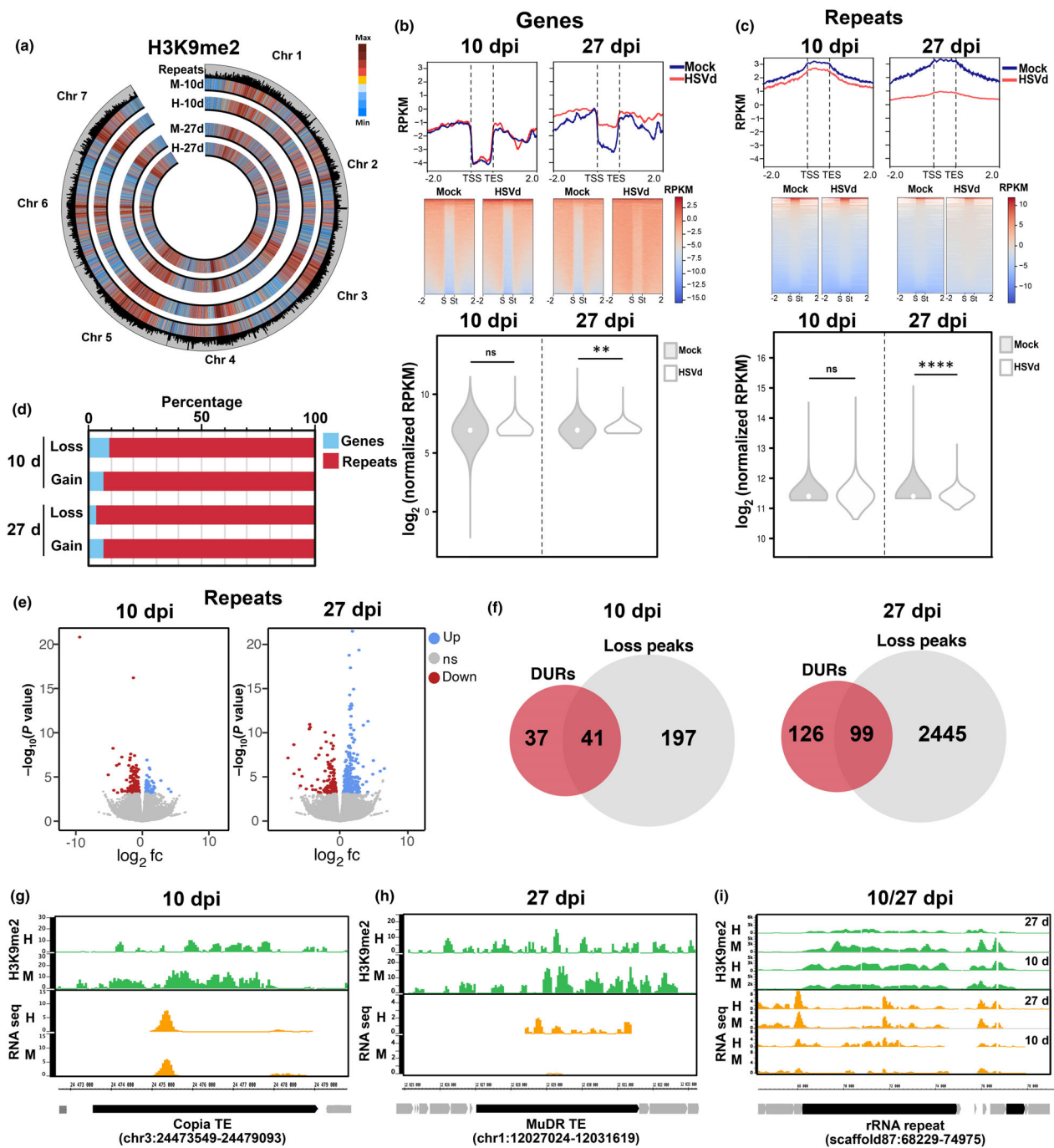


**Fig. 2** H3K9me2 dynamics under HSVd infection. (a) Circular plot showing the genome-wide levels of H3K9me2 in mock (M) and HSVd-infected (H) samples at 10 and 27 dpi (10 d and 27 d). The outermost track indicates the location and length of the repeats present in the *Cucumis sativus* genome. (b, c) Histone modification coverage profiles for genes (b) and repeats (c) in mock and HSVd-infected samples at 10 and 27 dpi. Graphs represent a 2 kb window (lower units) from the transcriptional start site (TSS) and the transcriptional end site (TES). Heatmaps of the values used for the profile graphs are also shown with the transcriptional start site indicated as 'S' and the transcriptional end site indicated as 'St'. Profiles are accompanied by a violin plot depicting the distribution of the  $\log_2$  transformed normalized RPKM values and the statistical significance of their difference. ns, nonsignificant, \*\* and \*\*\*\* indicate a  $P$ -value smaller than 0.01 and 0.001, respectively.  $P$ -values were calculated through an unpaired  $t$ -test. (d) Percentage of genes (blue) and repeats (red) present in loss or gain peaks identified at each of the time points analyzed. 10 d; 27 d. (e) Volcano plots showing differentially expressed repeats at 10 and 27 dpi. (f) Venn diagrams showing the overall overlap between 10 and 27 dpi differentially upregulated repeats (DURs) and repeats located at an H3K9me2 loss peak. (g–i) Genome browser screenshots showing examples of significantly upregulated repeats located at peaks losing H3K9me2 that experience transcriptional reactivation, including TEs from the Copia (g) and MuDR (h) superfamilies, and rRNA repeats (i). H3K9me2 values are indicated in green and RNA-Seq values are shown in orange. Note that rRNA transcriptional activation is not captured with regular RNA-Seq since rRNA transcripts are not polyadenylated. The time point of the identified overlap between H3K9me2 loss and transcriptional reactivation is shown on upper panel of the screenshot.

repeats compared to genes indicated again its preferential accumulation at heterochromatic regions and a redistribution of this mark from repeats to genes during HSVd infection (Fig. 2b). The accumulation changes observed showed that infected plants experienced a reorganization of heterochromatin under HSVd infection at later time points, while this mark was not significantly affected at earlier time points. Next, we predicted H3K9me2 peaks in both mock and infected tissues and explored the gain or loss of peaks of this mark in both conditions and time points (Fig. 2d; Table S2). As expected from the preferential heterochromatic nature of this mark, the majority of peaks were located at repeats (94% on average), pointing to the main role of this mark in the control of TEs and other repeats (Fig. 2d). To explore this role in regulating the transcription of repeats, we re-analyzed transcriptomic data obtained at identical time points from a previous work (Marquez-Molins *et al.*, 2023). In line with the potential role of H3K9me2 in the transcriptional control of repeats, cucumber plants experienced a transcriptional reactivation of repeats at both time points, with a higher number of differentially upregulated repeats (DURs) at later time points (78 and 225 significantly expressed repeats at 10 and 27 dpi, respectively, adjusted *P*-value < 0.05, Fig. 2e; Table S3). Interestingly, reactivated repeats overlapped with H3K9me2 changes during infection, since 53% and 44% of the reactivated repeats at 10 and 27 dpi, respectively, were within regions that lose H3K9me2 (Fig. 2f).

Targets of this reorganization include several TEs from the Copia (Fig. 2g) and MuDR superfamilies (Fig. 2h). Importantly, we also observed a reorganization of H3K9me2 at rRNA repeats that is significant at the later infection point (Figs 2i, S5A), which correlated with the reported transcriptional reactivation of these elements (Fig. S5B, note that rRNA genes are transcribed by Pol I and not polyadenylated, so RNA-Seq in this case shows an approximation of their actual expression level). HSVd is known to induce changes in the DNA methylation levels of ribosomal DNA repeats which correlates with a reactivation of its transcription (Martinez *et al.*, 2014; Castellano *et al.*, 2015, 2016a; Marquez-Molins *et al.*, 2023). Our analysis points to a potential relationship between our previously observed DNA methylation changes at rDNA repeats and the reorganization of H3K9me2 during HSVd infection, since both marks are intrinsically connected in cucumber (Fig. 1h). Despite this, the majority of H3K9me2 changes identified were not connected to changes in DNA methylation values at those regions, since almost all peaks retained similar DNA methylation values between mock and infected samples (the exception being CHH values in H3K9me2 gain peaks at 10 dpi which significantly decreased, Fig. S5C) indicating that neither RdDM activity or demethylation were driving H3K9me2 reorganization.

Second, H3K27me3 followed a mild reorganization under HSVd infection (Fig. 3a). At the genome-wide level, this mark showed significant enrichment in genes only at the earlier infection time point (Fig. 3b), while it was significantly lost from repeats at both 10 and 27 dpi (Fig. 3c). Similar to our H3K9me2 analysis, we predicted H3K27me3 peaks in both mock and infected tissues and explored the gain or loss of peaks

of this mark in both conditions and time points (Fig. 3d; Table S4). Compared to H3K9me2 (6% on average, Fig. 2d), H3K27me3 peaks are more frequent at genic locations (24% on average, Fig. 3d). Despite the presence of some of the peaks at repeat locations, their overall values (Fig. 3c) indicate that the presence of this mark at repeats is anecdotal. As expected, changes observed for this mark are independent of DNA methylation (Fig. S5D).

To further confirm these changes and to visualize the changes in their distribution at the subcellular level, we performed immunolocalization analyses in both mock and infected tissues at both infection time points (Fig. 4). Our results confirmed our genome-wide analysis for both marks. We observed a general reorganization of H3K9me2, which during HSVd infection experienced an expansion of its detection outside of the heterochromatic chromocenters (Fig. 4a), especially at 27 dpi (Fig. 4b), correlating with its increased presence at genes at later infection points. On the other hand, H3K27me3 did not show a change in its localization (Fig. 4a), but experienced a decrease in its overall intensity which was higher at 27 dpi (Fig. 4c). Overall, HSVd infection induced a reorganization of constitutive heterochromatin that was connected to the transcriptional reactivation of repeats, including TEs and rRNA genes, but disconnected from DNA methylation changes for a majority of its targets. These changes were also observed for facultative heterochromatin but at a lower intensity.

### H3K9me2 and H3K27me3 retain constitutive and facultative heterochromatic identity during viroid infection

We focused on understanding the dynamics of both heterochromatic marks under HSVd infection. First, we analyzed the dynamics of our predicted gain and loss peaks (Fig. 5a). Overall, on average, 20% of H3K9me2 and 31% of H3K27me3 peaks showed a dynamic nature (gain or loss of the peak under HSVd infection) while the rest (80% and 69% of the H3K9me2 and H3K27me3 peaks, respectively) remained stable. Following their main occupancy preference, gain and loss of the marks took place in centromeric/pericentromeric regions (for H3K9me2) and the arms of the chromosomes for H3K27me3 (Fig. 5b).

H3K9me2 and H3K27me3 are the main histone marks delimiting plant heterochromatin (Fransz *et al.*, 2006). In Arabidopsis, H3K27me3 can 'invade' constitutive heterochromatic regions under heavy loss of DNA methylation and/or heterochromatic identity in mutants, or under viral stress (Rougee *et al.*, 2021; Zhao *et al.*, 2022; Annacondia *et al.*, 2023). Interestingly, despite the overall reprogramming of the two marks observed during viroid infection (Figs 2–4), there was a minimal interaction (if any) between the loss and gain of any of the repressive histone marks, that was limited to a small overlap between H3K9me2 loss and H3K27me3 gain at 10 dpi (2.8% of the H3K9me2 loss peaks) and H3K9me2 gain and H3K27me3 loss at 10 dpi (0.4% of the H3K9me2 gain peaks) (Fig. 5c,h). Conservation of H3K9me2 and H3K27me3 peaks between the two time points (Fig. S6A,B, respectively) indicated that in both cases gain peaks were conserved to a higher degree than loss peaks. 24% of the H3K9me2

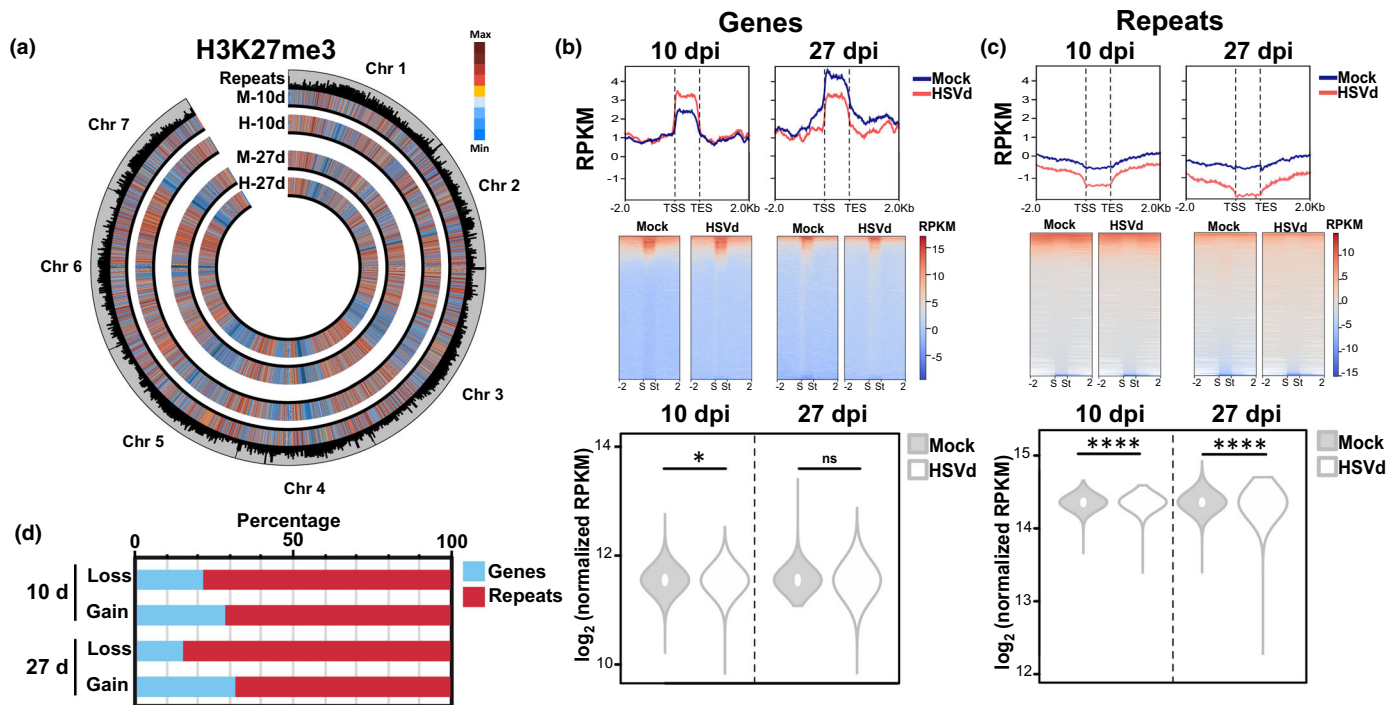


**Fig. 3** H3K27me3 dynamics under HSVd infection. (a) Circular plot showing the genome-wide levels of H3K27me3 in mock (M) and HSVd-infected (H) samples at 10 and 27 dpi. The outermost track indicates the location and length of the repeats present in the *Cucumis sativus* genome. (b, c) Histone modification coverage profiles for genes (b) and repeats (c) in mock and HSVd-infected samples at 10 and 27 dpi. Graphs represent a 2 kb window (lower units) from the transcriptional start site (TSS) and the transcriptional end site (TES). Heatmaps of the values used for the profile graphs are also shown with the transcriptional start site indicated as 'S' and the transcriptional end site indicated as 'St'. Profiles are accompanied by a violin plot depicting the distribution of the  $\log_2$  transformed normalized RPKM values and the statistical significance of their difference. ns, nonsignificant, \* and \*\*\*\* indicate a *P*-value smaller than 0.05 and 0.001, respectively. *P*-values were calculated through an unpaired *t*-test. (d) Percentage of genes (blue) and repeats (red) present in loss or gain peaks identified at each of the time points analyzed. 10 d; 27 d.

gain peaks at 27 dpi were conserved from the 10 dpi time point (Fig. S6A), while 15% of H3K27me3 peaks at 27 dpi were conserved from 10 dpi (Fig. S6B). On the other hand, only 1.2% of the H3K9me2 loss peaks at 27 dpi were conserved from the 10 dpi time point (Fig. S6A), and 1.9% of the H3K27me3 loss peaks at 27 dpi were preset at 10 dpi (Fig. S6B). Differences in the loss of H3K27me3 between the two time points correlate with the low correlation of the transcriptomic response between both time points previously observed (Marquez-Molins *et al.*, 2023).

Analysis of the accumulation values for both marks showed interesting trends. First, at both analyzed times, H3K9me2 was gained in regions with average/low values of the mark (Fig. 5d,f), while it was lost at locations showing a higher enrichment (Fig. 5e,g). This result correlated with our observed effect of H3K9me2 loss over the transcriptional reactivation of repeats (which are located at H3K9me2-rich regions). On the other hand, H3K27me3 was gained (although at lower levels) at regions with high values of the mark (Fig. 5i,k), while it was lost at regions with low values (Fig. 5j,l). Therefore, the reorganization of heterochromatin under HSVd infection was limited to regions with an already heterochromatic identity, and the gain (in opposition to the loss) of both marks was conserved at the two time points analyzed.

### Changes in gene expression correlate with H3K27me3 gain

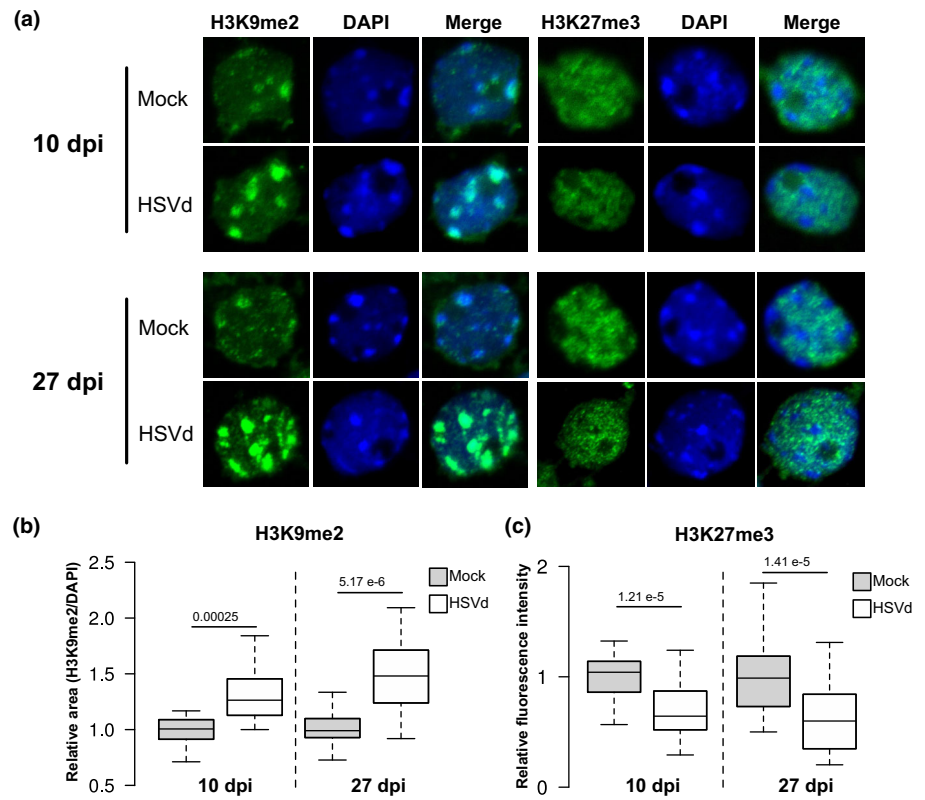
Next, we aimed to understand the influence of H3K9me2 and H3K27me3 reorganization on the genic transcriptional response to HSVd infection. First, we analyzed the overlap of genes with peaks showing a dynamic behavior under infection. We restricted our analysis to (1) genes directly associated with the gain or loss of H3K27me3 within their gene bodies, and (2) genes that gained or lost H3K9me2 within their gene bodies and a  $\pm 1$  kb window from their gene bodies.

Using this strategy, we identified 310 and 1221 genes with expression associated with changes in H3K9me2 and H3K27me3 marks, respectively (Fig. 6a; Table S5). Most of the genes (67% and 79%, for H3K9me2 and H3K27me3, respectively) were associated with gain peaks. To understand the role of genes regulated by repressive histone marks we explored their gene ontology (GO) classification. Genes overlapping with these marks were mainly associated with DNA, protein, and RNA binding categories, and with the transferase, hydrolase, and catalytic activities categories (Fig. 6b). Interestingly, some of these categories were preferentially associated with each of the marks. For example, DNA binding and kinase activity were predominantly associated with H3K27me3, while hydrolase and catalytic activities were in general related to H3K9me2 (Fig. 6b). Next, we



**Fig. 4** Immunolocalization of H3K9me2 and H3K27me3 in mock and HSVd-infected tissues.

(a) Representative images of H3K9me2 and H3K27me3 immunostained nuclei from mock and HSVd-infected *Cucumis sativus* leaves at 10 and 27 d postinfection (dpi). DAPI was used as a DNA counterstain that marks chromocenters and are a reference of the location of constitutive heterochromatin. Merge of the GFP and DAPI channels is shown to indicate the overlap of both signals. (b) Box plot showing the values of H3K9me2 signal area relative to the DAPI signal area. *P*-value for the comparisons between mock and HSVd is shown on upper panel of the corresponding box plots. Values for both 10 and 27 d postinfection (dpi) as indicated are shown. (c) Box plot showing the values of H3K27me3 signal intensity are shown. *P*-value for the comparisons between mock and HSVd is shown on upper panel of the corresponding box plots. Values for both 10 and 27 d postinfection (dpi) as indicated are shown. *P*-values were calculated through an unpaired *t*-test. All boxplots are Tukey's style (whiskers extend to data points that are  $< 1.5 \times$  IQR away from the 1<sup>st</sup>/3<sup>rd</sup> quartile).



explored the influence of the presence of gain or loss peaks over the transcriptional activation or repression of gene expression in response to HSVd infection. To that end, we used transcriptional data from previous experiments at analogous time points to infer the expression level of the genes located within histone peaks. Our analysis indicated that from the different marks and their respective environments, only the gain of H3K27me3 (significant gain peaks during HSVd infection) overlapped with an overall significant decrease of the expression of all its target genes at both analyzed time points (Fig. 6c). This result is in line with the known repressive role of this histone mark and shows its dynamism during HSVd infection and its role in the control of gene expression.

Several differentially expressed genes (DEGs, 26 at 10 dpi and 28 at 27 dpi) were found associated with H3K27me3 changes, with both gain (23 at 10 dpi and 18 at 27 dpi) and loss (3 at 10 dpi and 10 at 27 dpi) of marks (Fig. 6d; Table S5). Interestingly, the gain of H3K27me3 took place at genes with already high values of H3K27me3 (Fig. 6e). By contrast, loss of this mark took place at genes with medium/low values of the mark, indicating that this mark is not gained *de novo* but rather, reinforced at previous heterochromatic locations (Fig. 6g). DEGs associated with H3K27me3 peaks included genes potentially involved in the mediation of the stress response. For example, expression of calmodulin binding (CsaV3\_1G038380) and acyl-transferase activity (CsaV3\_3G027830) genes (associated with H3K27me3 gain, Fig. 6f) or an oxidoreductase (CsaV3\_3G033740) and transcription factor (CsaV3\_5G004600) genes (connected to H3K27me3 loss, Fig. 6h). Additionally, certain DEGs (4 at 10 dpi and 1 at

27 dpi) were also associated with H3K9me2 changes, including CsaV3\_7G025330, a bystin-like protein, potentially involved in cell proliferation (Wang *et al.*, 2009; Carron *et al.*, 2011) (Fig. S7A), and CsaV3\_7G015110, a homolog of the enhanced downy mildew 2 protein, a NLS protein that may regulate RPP7 expression (Lai *et al.*, 2020) (Fig. S7B), which has previously been proposed to be epigenetically regulated by heterochromatin in *Arabidopsis* (Duan *et al.*, 2017). Overall, our data indicate a potential role of histone marks in the regulation of the transcriptional response to HSVd infection with a correlation of H3K27me3-mediated repression and downregulated genes, and a potential minor contribution of H3K9me2 in the control of gene expression.

## Discussion

Epigenetic regulation plays an important role in the adaptation of the transcriptional program to external signals that determine plant development (He *et al.*, 2012; Gan *et al.*, 2015; Cheng *et al.*, 2020; Shen *et al.*, 2021; Kim *et al.*, 2023). Stress associated with adverse environmental conditions has been identified as yet another stimulus that can induce epigenetic changes in plants (Probst & Scheid, 2015; Lamke & Baurle, 2017; Annacondia *et al.*, 2018). Several studies have identified dynamic DNA methylation changes upon stress exposure, but the role of histone marks in this context has remained unexplored. In this work, we have studied the dynamism and role of the two main repressive histone marks (H3K9me2 and H3K27me3) in the modulation of the transcriptional response against viroid infection. Our data

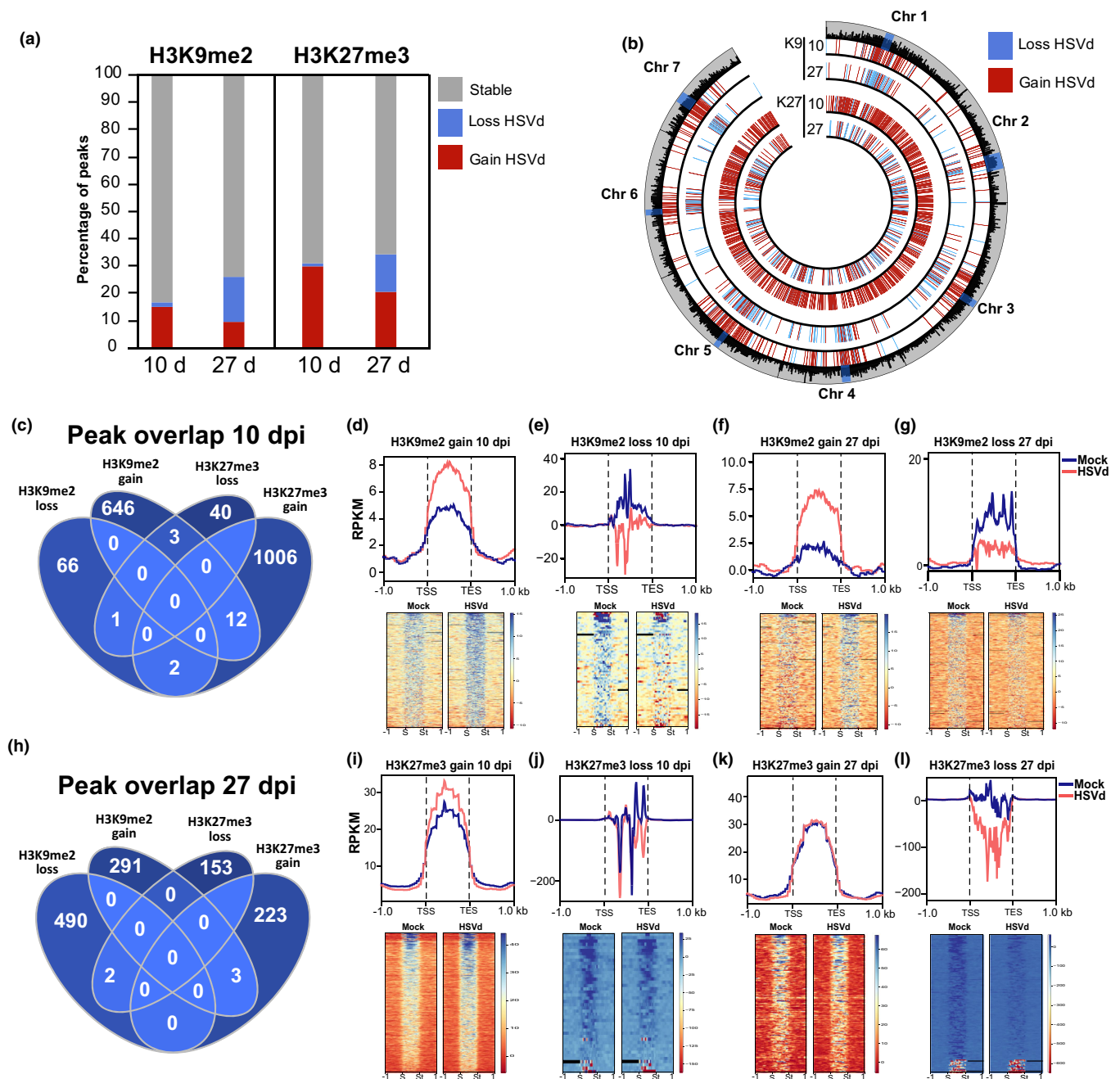


**Fig. 5** Genome-wide analysis of H3K9me2 and H3K27me3 changes under HSVd infection. (a) Analysis of the dynamism of the peaks identified under HSVd infection for both H3K9me2 and H3K27me3. Stable peaks were identified in both mock and HSVd-infected samples, while loss and gain peaks were only identified in mock or HSVd-infected samples, respectively. 10 d; 27 d. (b) Circular plot showing the genome-wide location of the identified loss and gain histone peaks for both H3K9me2 (K9) and H3K27me3 (K27) samples at both 10 (10) and 27 (27) dpi. The outermost track indicates the location and length of the repeats present in the *Cucumis sativus* genome. The location of centromeres according to the cytogenetic analysis from Sun *et al.* (2013) is shown in blue. (c) Venn diagram showing the overlap between the H3K9me2 and H3K27me3 gain and loss peaks at 10 dpi. (d–g) Histone modification coverage profiles for the identified H3K9me2 peaks in mock and HSVd-infected samples at 10 and 27 dpi. Profiles show: H3K9me2 (K9) gain peaks at 10 dpi (d), H3K9me2 loss peaks at 10 dpi (e), H3K9me2 gain peaks at 27 dpi (f), H3K9me2 loss peaks at 27 dpi (g). Graphs represent a 2 kb window (lower units) from the transcriptional start site (TSS) and the transcriptional end site (TES). Heatmaps of the values used for the profile graphs are also shown with the transcriptional start site indicated as 'S' and the transcriptional end site indicated as 'St'. (h) Venn diagram showing the overlap between the H3K9me2 and H3K27me3 gain and loss peaks at 27 dpi. (i–l) Histone modification coverage profiles for the identified H3K27me3 peaks in mock and HSVd-infected samples at 10 and 27 dpi. Profiles show: H3K27me3 (K27) gain peaks at 10 dpi (i), H3K27me3 loss peaks at 10 dpi (j), H3K27me3 gain peaks at 27 dpi (k), H3K27me3 loss peaks at 27 dpi (l). Graphs represent a 2 kb window (lower units) from the transcriptional start site (TSS) and the transcriptional end site (TES). Heatmaps of the values used for the profile graphs are also shown with the transcriptional start site indicated as 'S' and the transcriptional end site indicated as 'St'.

shows that heterochromatic histone marks are reorganized during HSVd infection, with a major role of H3K27me3 gain in the repression of gene expression.

Our work adds yet another piece of evidence to the role of histone marks in the control of transcription and genome stability in response to stress conditions. Histone marks and chromatin structure were previously identified in forward genetic analysis as major players in the control of the stress response (Agorio & Vera, 2007; López *et al.*, 2011; Yu *et al.*, 2013). Despite this identification, genome-wide information on their role and targets was largely missing. Our analysis contributes to the overall understanding of the organization of epigenomic information during stress. Additionally, we provide information on the role of these epigenetic mechanisms in an economically relevant crop, *Cucumis sativus*, advancing our knowledge of the conservation of their role in nonmodel plant species.

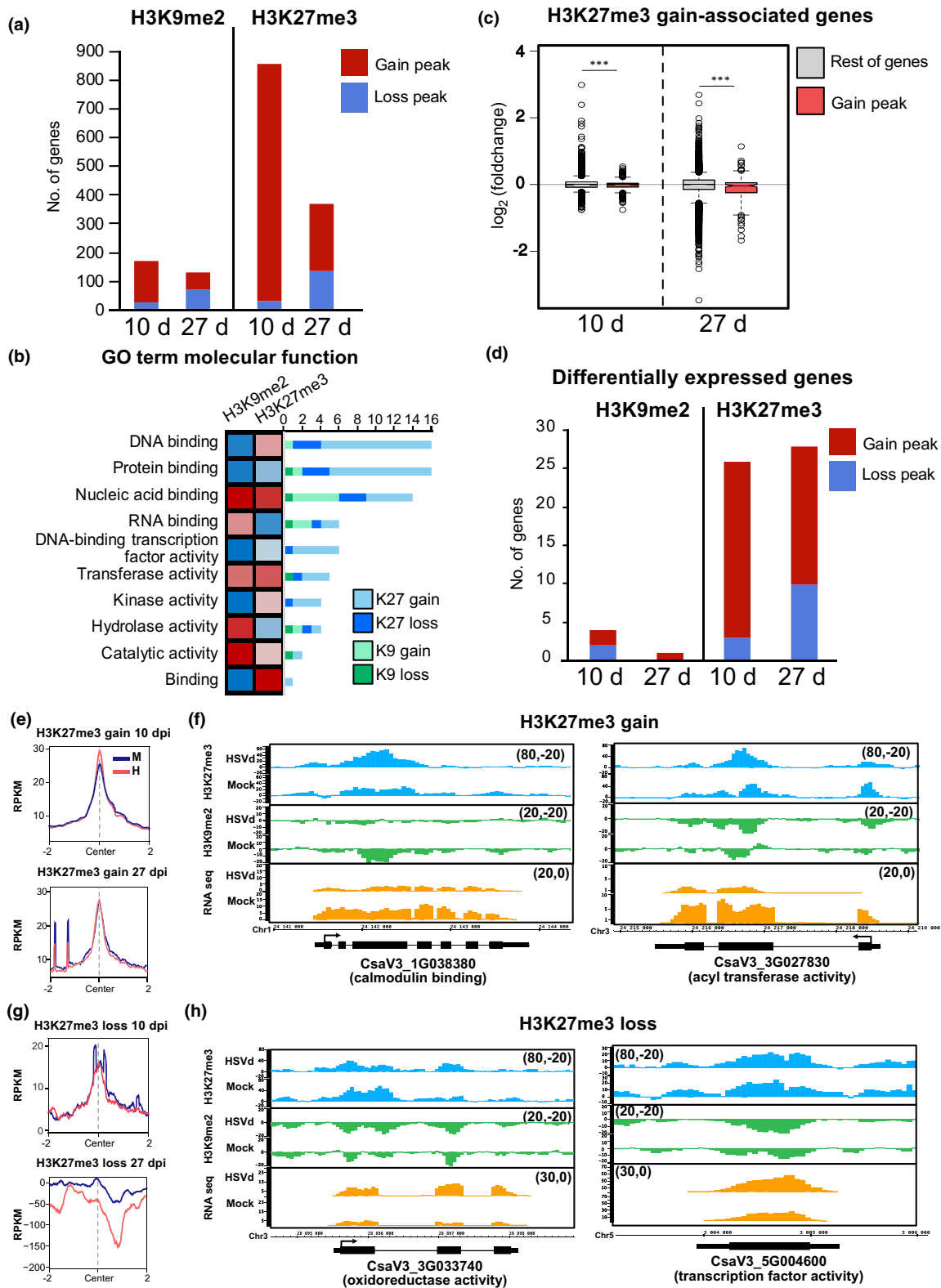
We show that the organization of repressive histone marks in the cucumber genome (Fig. 1a) resembles their previously described distribution in *Arabidopsis* (Roudier *et al.*, 2011), melon (Latrasse *et al.*, 2017; Pichot *et al.*, 2022), and *Physcomitrella patens* (Widiez *et al.*, 2014), with H3K9me2 marking constitutive heterochromatin (located at the chromosomal centromeric regions, Fig. 1a,c,d) and H3K27me3 featuring facultative heterochromatin (spaced through the chromosome arms Fig. 1a,b,d). Our results also correlate with previous cytogenetic analyses of cucumber chromatin (Sun *et al.*, 2013). In line with this preferential accumulation, H3K27me3 and H3K9me2 are highly enriched at genes and repeats, respectively (Fig. 1b,c). Similar to *Arabidopsis*, H3K9me2 in cucumber is also correlated with the presence of DNA methylation, since H3K9me2 enriched regions showed high values of cytosine methylation in all sequence contexts (Fig. 1h). This points to a connection between the RdDM pathway and H3K9me2 homeostasis in cucumber, similar to the one inferred from the genetic analysis of CMT3 and KYP mutants in tomato (Wang & Baulcombe, 2020) and pointing to the conservation of that connection in angiosperms. On the other hand, DNA methylation and H3K27me3 are negatively correlated in cucumber (Figs 1h, S4E), similar to its known distribution in other species such as *Arabidopsis* (Cokus *et al.*, 2008; Law & Jacobsen, 2010; Liu *et al.*, 2021).

HSVd infection induces a global reorganization of cucumber heterochromatin. This reorganization is characterized, first, by a progressive reduction of H3K9me2 from repeats (Fig. 2c) and an increase at genes (Fig. 2b), a dynamism that we could observe also at the subcellular level (Fig. 4a,b). Second, H3K27me3 shows an initial increase followed by a decrease of H3K27me3 from genes (Fig. 3b) and an overall loss from repeats (Fig. 3c), a response that also correlates with our immunolocalization analysis (Fig. 4a,c). Changes in the presence of both histone marks are influenced by the previous presence of those marks at the enriched peaks, with most of the gain and loss of H3K9me2 and H3K27me3 gain taking place at regions already enriched on that particular mark (Fig. 5d,f,i,k). In line with this accumulation pattern and the canonical role of both repressive marks, repeats are transcriptionally reactivated at later infection points (Fig. 2g), while genes are mostly affected by the gain of

H3K27me3 (Fig. 6c). Transcriptional reactivation of repeats has been connected to genome reorganization induced by TE activity (Cavrak *et al.*, 2014; Ito *et al.*, 2016; Roquis *et al.*, 2021) and the reprogramming of the transcriptional response to stress (Deneveth *et al.*, 2022). Recently, TE activity has been linked to the transition from bisexual to unisexual flowering types in cucurbits (Huang *et al.*, 2024). Whether a similar TE activity might play a role in the reorganization of gene structure or activity during virioid infection is an attractive hypothesis. On the other hand, H3K27me3 loss seems to take place only in regions with low values of that mark (Fig. 5j,l) and is enriched at DEGs (Fig. 6d). Similar results on the overlap of the connection between gene expression and H3K27me3 reorganization were recently obtained in virus-infected plants, where a catalytic component of the PRC2 complex (CURLY LEAF) was identified as a factor promoting viral tolerance (Annacondia *et al.*, 2023). Our result is in line with the known role of H3K27me3 in the regulation of both the stress response (Widiez *et al.*, 2014; Dvorak Tomastikova *et al.*, 2021) and developmental cues (He *et al.*, 2012; Gan *et al.*, 2015; Moreno-Romero *et al.*, 2019; Batista & Kohler, 2020; Cheng *et al.*, 2020; Shen *et al.*, 2021; Kim *et al.*, 2023).

Previous analysis of the interaction between the repressive histone marks H3K9me2 and H3K27me3 have identified a compensatory mechanism where H3K27me3 invades H3K9me2 regions in mutant backgrounds that lose constitutive heterochromatin (Rougee *et al.*, 2021; Zhao *et al.*, 2022) or under CMV infection (Annacondia *et al.*, 2023). Here we were not able to identify a similar mechanism, and indeed, despite the strong symptomatology displayed by plants infected with HSVd (similar to CMV), the two heterochromatic marks retained their identity (Fig. 5c,h). Further analysis under different/stronger stresses would be needed to assess if H3K9me2/H3K27me3 compensatory activity is exclusive of the *A. thaliana* genome or is also present in other plant genomes. It might be possible that the differences in genome structure, genome size (367 Mb compared to 135 Mb for the *A. thaliana* genome) and/or the activity of other uncharacterized compensatory repressive epigenetic marks in cucumber determine this difference with the homologous mechanism from *Arabidopsis*.

Lastly, we correlated the observed changes in repressive histone marks to the transcriptional changes previously associated with HSVd infection (Marquez-Molins *et al.*, 2023). This analysis indicated that, as expected (Roudier *et al.*, 2011), H3K27me3 is vastly more associated with genes than H3K9me2 (Fig. 6a). Nevertheless, we identified some genes whose expression correlates with the presence of enriched or depleted regions for each of the histone marks. Additionally, some of the gene categories seem to be preferentially associated with each of the two repressive histone marks (Fig. 6b). This observation is in line with the known roles of H3K27me3 in regulating the sensing of environmental signals (Zhang *et al.*, 2007) and a potential role of H3K9me2 in the control of housekeeping metabolic activities as observed in other species such as *C. elegans* or humans (Lee *et al.*, 2019; Wu *et al.*, 2023). Further analysis of the connection between histone marks and particular gene families/categories should be carried



out to confirm this observation. Additionally, compared to H3K9me2, H3K27me3 is preferentially associated with DEGs (Fig. 6d), supporting the role of this mark in transcriptional

reprogramming under HSVd infection. Indeed we identified several genes associated with the gain or loss of this mark that might be important regulators of HSVd defense response, including a

**Fig. 6** H3K27me3 and H3K9me2 contribute to the transcriptional reprogramming under HSVd infection. (a) Histogram showing the total number of genes located at gain (red) and loss (blue) peaks for H3K9me2 and H3K27me3 at 10 and 27 dpi (10 d and 27 d). (b) Gene ontology (GO) categorization by molecular function for the categories indicated of the genes showing association with either H3K9me2 or H3K27me3 peaks. The heatmap shows the enrichment of the terms for peaks identified as associated with either H3K9me2 or H3K27me3 peaks. Histogram showing the number of genes associated with gain or loss peaks for each of the histone marks analyzed. (c) Expression values ( $\log_2$  (fold change)) for all genes associated with H3K27me3 gain peaks at 10 and 27 dpi (10 d and 27 d, colored in red) compared to the rest of the genes (all genes with expression in the *Cucumis sativus* genome with the subtracted values for peak-associated genes). *P*-values are indicated on upper of each comparison and were calculated through an unpaired *t*-test. \*\*\*, *P*-value lower than 0.005. Boxplots are Tukey's style (whiskers extend to data points that are  $< 1.5 \times$  IQR away from the 1<sup>st</sup>/3<sup>rd</sup> quartile). (d) Histogram showing the total number of differentially expressed genes located at gain (red) and loss (blue) peaks for H3K9me2 and H3K27me3 at 10 and 27 dpi. (e) H3K27me3 coverage profiles for H3K27me3 gain peaks in mock (M) and HSVd-infected (H) samples at 10 (upper panel) and 27 (lower panel) dpi. Graphs represent a 2 kb window (lower units) from the center of the region. (f) Genome browser screenshots showing examples of significantly downregulated genes (significantly differentially expressed) located at peaks gaining H3K27me3. H3K27me3 values are shown in blue, H3K9me2 values are shown in green and RNA-Seq values are shown in orange. Higher and lower values of the track are indicated in the brackets. (g) H3K27me3 coverage profiles for H3K27me3 loss peaks in mock (M) and HSVd-infected (H) samples at 10 (upper panel) and 27 (lower panel) dpi. Graphs represent a 2 kb window (lower units) from the center of the region. (h) Genome browser screenshots showing examples of significantly upregulated genes (significantly differentially expressed) located at peaks losing H3K27me3. H3K27me3 values are shown in blue, H3K9me2 values are shown in green and RNA-Seq values are shown in orange. Higher and lower values of the track are indicated in the brackets.

calmodulin-binding gene, which mediates the first wave of plant responses to multiple stresses through  $\text{Ca}^{2+}$  binding (Snedden & Fromm, 1998; Yang & Poovaiah, 2003; Zeng *et al.*, 2015), an acyl-transferase gene, which are known to affect plant growth (Smotrys & Linder, 2004; Li *et al.*, 2022), an oxidoreductase activity gene, known for controlling oxidative stress in plants (Saha *et al.*, 2016), or a transcription factor, among other DEGs (Fig. 6f,h).

How could a minimal pathogen such as a viroid induce these dramatic changes in histone homeostasis? We envision that this interaction might be indirect, due to the transcriptomic reprogramming needed to cope with the infection, or direct, through interaction with components of histone homeostasis (Fig. S8). HSVd is a member of the *Pospiviroidae* family, characterized by its ability to replicate in the nucleus. It is plausible that the accumulation of HSVd in the nucleus alters the homeostasis of that organelle environment, inducing changes in the epigenetic regulation of the genome at its core, the structure of the chromatin. Indeed, HSVd interacts with HDA6, a histone deacetylase that is needed to enhance DNA methylation mediated by MET1 and histone modifications mediated by the histone demethylase FLD (an LSD1 homolog) (Aufsatz *et al.*, 2002; Liu *et al.*, 2012). FLD functions as an activator of flowering through the repression of FLC, which is controlled by H3K27me3 (He *et al.*, 2003). This interaction with histone homeostasis could lead to the increased values of H3K27me3, which seems of particular importance under HSVd infection-induced transcriptional reprogramming. Indeed, HSVd-infected plants show a delay in flowering time (Martínez *et al.*, 2008), which could be connected to our observed H3K27me3 reorganization. Since in our analyses, the changes observed at H3K9me2 peaks were independent of any DNA methylation change, we disfavor that HSVd interactions with histone modifications is a consequence of the interference of HSVd-derived siRNAs with the RdDM pathway and, consequently, H3K9me2 homeostasis. To summarize, our work adds data supporting the role of epigenomic reprogramming, particularly heterochromatin reorganization, playing an active role in the transcriptional reprogramming experienced under viroid infection. Moreover, our results expand our understanding of the complex interaction between viroids and their hosts.

## Acknowledgements

We thank all members of the Martínez and Gómez labs for their valuable comments on the manuscript. Sequencing was performed by Novogene (United Kingdom). The data handling was performed using UPPMAX which is part of the Swedish National Infrastructure for Computing (SNIC). We thank Formas (2021-01161), the Swedish Research Council (VR 2021-05023), and the Knut and Alice Wallenberg Foundation (KAW 2019.0062) for supporting research in the Martínez group, and The Knowledge Generation Program of the Spanish Research Agency (PID2022\_1393930B-I00) in the Gómez group. Open Access funding is provided by the Swedish University of Agricultural Sciences. The data handling was enabled by resources provided by the Swedish National Infrastructure for Computing (SNIC) at UPPMAX partially funded by the Swedish Research Council through grant agreement no. 2018-05973.

## Competing interests

None declared.

## Author contributions

JM-M: Formal analysis, Methodology, Validation, Writing – review & editing. JC: Formal analysis, Methodology, Validation, Writing – review & editing. JC-S: Bioinformatic Analysis. VTJ-G: Formal analysis, Methodology, Bioinformatic Analysis, Writing – review & editing. PV-B: Bioinformatic Analysis. MLA: Formal analysis, Methodology, Validation, Writing – review & editing. GG: Conceptualization, Formal analysis, Writing – review & editing. GM: Conceptualization, Formal analysis, Methodology, Validation, Bioinformatic Analysis, Writing – original draft. JM-M and JC contributed equally to this work.

## ORCID

Maria Luz Annacondia  <https://orcid.org/0000-0001-7998-8362>

Jinping Cheng  <https://orcid.org/0000-0003-0749-7649>

Julia Corell-Sierra  <https://orcid.org/0000-0003-0751-4381>  
 Gustavo Gomez  <https://orcid.org/0000-0003-3715-7792>  
 Vasti Thamara Juarez-Gonzalez  <https://orcid.org/0000-0002-2631-8928>  
 Joan Marquez-Molins  <https://orcid.org/0000-0002-6487-6488>  
 German Martinez  <https://orcid.org/0000-0002-5215-0866>  
 Pascual Villalba-Bermell  <https://orcid.org/0000-0001-6057-6755>

## Data availability

All raw and processed sequencing data generated in this study have been submitted to the NCBI Gene Expression Omnibus (GEO; <https://www.ncbi.nlm.nih.gov/geo/>) under accession no.: GSE249651.

## References

- Afgan E, Baker D, Batut B, van den Beek M, Bouvier D, Čech M, Chilton J, Clements D, Coraor N, Grüning BA *et al.* 2018. The Galaxy platform for accessible, reproducible and collaborative biomedical analyses: 2018 update. *Nucleic Acids Research* 46: W537–W544.
- Agorio A, Vera P. 2007. ARGONAUTE4 is required for resistance to *Pseudomonas syringae* in Arabidopsis. *Plant Cell* 19: 3778–3790.
- Alvarez-Venegas R, Al Abdallat A, Guo M, Alfano JR, Avramova Z. 2007. Epigenetic control of a transcription factor at the cross section of two antagonistic pathways. *Epigenetics* 2: 106–113.
- Annacondia ML, Juarez-Gonzalez VT, Cheng J, Reig-Valiente JL, Martinez G. 2023. Heterochromatin re-organization associated with the transcriptional reprogramming under viral infection in Arabidopsis. *bioRxiv*. doi: 10.1101/2023.08.30.555647.
- Annacondia ML, Mageroy MH, Martinez G. 2018. Stress response regulation by epigenetic mechanisms: changing of the guards. *Physiologia Plantarum* 162: 239–250.
- Annacondia ML, Markovic D, Reig-Valiente JL, Scaltsoyiannes V, Pieterse CMJ, Ninkovic V, Slotkin RK, Martinez G. 2021. Aphid feeding induces the relaxation of epigenetic control and the associated regulation of the defense response in Arabidopsis. *New Phytologist* 230: 1185–1200.
- Aufsatz W, Mette MF, van der Winden J, Matzke M, Matzke AJM. 2002. HDA6, a putative histone deacetylase needed to enhance DNA methylation induced by double-stranded RNA. *EMBO Journal* 21: 6832–6841.
- Batista RA, Kohler C. 2020. Genomic imprinting in plants-revisiting existing models. *Genes & Development* 34: 24–36.
- Becker JS, McCarthy RL, Sidoli S, Donahue G, Kaeding KE, He Z, Lin S, Garcia BA, Zaret KS. 2017. Genomic and proteomic resolution of heterochromatin and its restriction of alternate fate genes. *Molecular Cell* 68: 1023–1037.
- Berr A, McCallum EJ, Alioua A, Heintz D, Heitz T, Shen WH. 2010. Arabidopsis histone methyltransferase SET DOMAIN GROUP8 mediates induction of the jasmonate/ethylene pathway genes in plant defense response to necrotrophic fungi. *Plant Physiology* 154: 1403–1414.
- Berriri S, Gangappa SN, Kumar SV. 2016. SWR1 chromatin-remodeling complex subunits and H2A.Z have non-overlapping functions in immunity and gene regulation in Arabidopsis. *Molecular Plant* 9: 1051–1065.
- Boyko A, Kathiria P, Zemp FJ, Yao Y, Pogribny I, Kovalchuk I. 2007. Transgenerational changes in the genome stability and methylation in pathogen-infected plants: (virus-induced plant genome instability). *Nucleic Acids Research* 35: 1714–1725.
- Cambiagno DA, Torres JR, Alvarez ME. 2021. Convergent epigenetic mechanisms avoid constitutive expression of immune receptor gene subsets. *Frontiers in Plant Science* 12: 703667.
- Carron C, O'Donohue MF, Choessel V, Faubladiere M, Gleizes PE. 2011. Analysis of two human pre-ribosomal factors, bystin and hTsr1, highlights differences in evolution of ribosome biogenesis between yeast and mammals. *Nucleic Acids Research* 39: 280–291.
- Castellano M, Martinez G, Marques MC, Moreno-Romero J, Kohler C, Pallas V, Gomez G. 2016a. Changes in the DNA methylation pattern of the host male gametophyte of viroid-infected cucumber plants. *Journal of Experimental Botany* 67: 5857–5868.
- Castellano M, Martinez G, Pallas V, Gómez G. 2015. Alterations in host DNA methylation in response to constitutive expression of Hop stunt viroid RNA in *Nicotiana benthamiana* plants. *Plant Pathology* 64: 1247–1257.
- Castellano M, Pallas V, Gomez G. 2016b. A pathogenic long noncoding RNA redesigns the epigenetic landscape of the infected cells by subverting host Histone Deacetylase 6 activity. *New Phytologist* 211: 1311–1322.
- Cavrak VV, Lettner N, Jamge S, Kosarewicz A, Bayer LM, Mittelsten Scheid O. 2014. How a retrotransposon exploits the plant's heat stress response for its activation. *PLoS Genetics* 10: e1004115.
- Chan C, Zimmerli L. 2019. The histone demethylase IBM1 positively regulates immunity by control of defense gene expression. *Frontiers in Plant Science* 10: 1587.
- Cheng K, Xu YC, Yang C, Ouellette L, Niu LJ, Zhou XC, Chu LT, Zhuang F, Liu J, Wu HL *et al.* 2020. Histone tales: lysine methylation, a protagonist in Arabidopsis development. *Journal of Experimental Botany* 71: 793–807.
- Choi SM, Song HR, Han SK, Han M, Kim CY, Park J, Lee YH, Jeon JS, Noh YS, Noh B. 2012. HDA19 is required for the repression of salicylic acid biosynthesis and salicylic acid-mediated defense responses in Arabidopsis. *The Plant Journal* 71: 135–146.
- Cokus SJ, Feng SH, Zhang XY, Chen ZG, Merriman B, Haudenschild CD, Pradhan S, Nelson SF, Pellegrini M, Jacobsen SE. 2008. Shotgun bisulphite sequencing of the Arabidopsis genome reveals DNA methylation patterning. *Nature* 452: 215–219.
- Coleman-Derr D, Zilberman D. 2012. Deposition of histone variant H2A.Z within gene bodies regulates responsive genes. *PLoS Genetics* 8: e1002988.
- Deneweth J, Van de Peer Y, Vermeirssen V. 2022. Nearby transposable elements impact plant stress gene regulatory networks: a meta-analysis in *A. thaliana* and *S. lycopersicum*. *BMC Genomics* 23: 18.
- Dhawan R, Luo HL, Foerster AM, AbuQamar S, Du HN, Briggs SD, Scheid OM, Mengiste T. 2009. HISTONE MONOUBIQUITINATION1 interacts with a subunit of the mediator complex and regulates defense against necrotrophic fungal pathogens in Arabidopsis. *Plant Cell* 21: 1000–1019.
- Di Serio F, Li SF, Matousek J, Owens RA, Pallas V, Randles JW, Sano T, Verhoeven JJJ, Vidalakis G, Flores R *et al.* 2018. ICTV virus taxonomy profile. *Journal of General Virology* 99: 611–612.
- Di Serio F, Owens RA, Li SF, Matousek J, Pallas V, Randles JW, Sano T, Verhoeven JJJ, Vidalakis G, Flores R *et al.* 2021. ICTV virus taxonomy profile. *Journal of General Virology* 102: jgv001543.
- Doucet D, Kellenberger RT, Schlüter PM, Schiestl FP. 2016. Herbivore-induced DNA demethylation changes floral signalling and attractiveness to pollinators in *Brassica rapa*. *PLoS ONE* 11: e0166646.
- Downen RH, Pelizzola M, Schmitz RJ, Lister R, Downen JM, Nery JR, Dixon JE, Ecker JR. 2012. Widespread dynamic DNA methylation in response to biotic stress. *Proceedings of the National Academy of Sciences, USA* 109: E2183–E2191.
- Duan CG, Wang XG, Zhang LR, Xiong XS, Zhang ZJ, Tang K, Pan L, Hsu CC, Xu HW, Tao WA *et al.* 2017. A protein complex regulates RNA processing of intronic heterochromatin-containing genes in Arabidopsis. *Proceedings of the National Academy of Sciences, USA* 114: E7377–E7384.
- Dutta A, Choudhary P, Caruana J, Raina R. 2017. JM27, an Arabidopsis H3K9 histone demethylase, modulates defense against and flowering time. *The Plant Journal* 91: 1015–1028.
- Dvorak Tomastikova E, Hafren A, Trejo-Arellano MS, Rasmussen SR, Sato H, Santos-Gonzalez J, Kohler C, Hennig L, Hofius D. 2021. Polycomb repressive complex 2 and KRYPTONITE regulate pathogen-induced programmed cell death in Arabidopsis. *Plant Physiology* 185: 2003–2021.
- Feng W, Michaels SD. 2015. Accessing the inaccessible: the organization, transcription, replication, and repair of heterochromatin in plants. *Annual Review of Genetics* 49: 439–459.

- Flores R, Hernández C, Martínez de Alba AE, Daròs JA, Di Serio F. 2005. Viroids and viroid-host interactions. *Annual Review of Phytopathology* 43: 117.
- Franz P, ten Hoopen R, Tessoro F. 2006. Composition and formation of heterochromatin in *Arabidopsis thaliana*. *Chromosome Research* 14: 71–82.
- Gan ES, Xu YF, Ito T. 2015. Dynamics of H3K27me3 methylation and demethylation in plant development. *Plant Signaling & Behavior* 10: e1027851.
- Gohlke J, Scholz CJ, Kneitz S, Weber D, Fuchs J, Hedrich R, Deeken R. 2013. DNA methylation mediated control of gene expression is critical for development of crown gall tumors. *PLoS Genetics* 9: e1003267.
- Hadley W. 2016. *GGPLOT2: elegant graphics for data analysis*. New York, NY, USA: Springer-Verlag.
- He CS, Chen XF, Huang H, Xu L. 2012. Reprogramming of H3K27me3 is critical for acquisition of pluripotency from cultured Arabidopsis tissues. *PLoS Genetics* 8: e1002911.
- He YH, Michaels SD, Amasino RM. 2003. Regulation of flowering time by histone acetylation in Arabidopsis. *Science* 302: 1751–1754.
- He Z. 2019. An H3K27me3 demethylase-HSFA2 loop controls thermomemory associated with attenuated immunity and early flowering in Arabidopsis. *Molecular Plant–Microbe Interactions* 32: 225.
- Hewezi T, Lane T, Piya S, Rambani A, Rice JH, Staton M. 2017. Cyst nematode parasitism induces dynamic changes in the root epigenome. *Plant Physiology* 174: 405–420.
- Hu Y, Lu Y, Zhao Y, Zhou DX. 2019. Histone acetylation dynamics integrates metabolic activity to regulate plant response to stress. *Frontiers in Plant Science* 10: 1236.
- Huang HY, Zhang S, Choucha FA, Verdenaud M, Tan FQ, Pichot C, Parsa HS, Slavkovic F, Chen Q, Troadec C *et al.* 2024. Harbinger transposon insertion in ethylene signaling gene leads to emergence of new sexual forms in cucurbits. *Nature Communications* 15: 4877.
- Huang Y, Sicar S, Ramirez-Prado JS, Manza-Mianza D, Antunez-Sanchez J, Briik-Chaouche R, Rodriguez-Granados NY, An J, Bergounioux C, Mahfouz MM *et al.* 2021. Polycomb-dependent differential chromatin compartmentalization determines gene coregulation in Arabidopsis. *Genome Research* 31: 1230–1244.
- Huot B, Yao J, Montgomery BL, He SY. 2014. Growth-defense tradeoffs in plants: a balancing act to optimize fitness. *Molecular Plant* 7: 1267–1287.
- Ito H, Kim JM, Matsunaga W, Saze H, Matsui A, Endo TA, Harukawa Y, Takagi H, Yaegashi H, Masuta Y *et al.* 2016. A stress-activated transposon in Arabidopsis induces transgenerational abscisic acid insensitivity. *Scientific Reports* 6: 23181.
- Jaskiewicz M, Conrath U, Peterhansel C. 2011. Chromatin modification acts as a memory for systemic acquired resistance in the plant stress response. *EMBO Reports* 12: 50–55.
- Kim J, Bordiya Y, Xi YP, Zhao B, Kim DH, Pyo Y, Zong W, Ricci WA, Sung SB. 2023. Warm temperature-triggered developmental reprogramming requires VIL1-mediated, genome-wide H3K27me3 accumulation in Arabidopsis. *Development* 150: dev201343.
- Lai Y, Lu XM, Daron J, Pan SQ, Wang JQ, Wang W, Tsuchiya T, Holub E, McDowell JM, Slotkin RK *et al.* 2020. The Arabidopsis PHD-finger protein EDM2 has multiple roles in balancing NLR immune receptor gene expression. *PLoS Genetics* 16: e1008993.
- Lamke J, Baurle I. 2017. Epigenetic and chromatin-based mechanisms in environmental stress adaptation and stress memory in plants. *Genome Biology* 18: 124.
- Latrasse D, Rodriguez-Granados NY, Veluchamy A, Mariappan KG, Bevilacqua C, Crapart N, Camps C, Sommar V, Raynaud C, Dogimont C *et al.* 2017. The quest for epigenetic regulation underlying unisexual flower development in *Cucumis melo*. *Epigenetics & Chromatin* 10: 22.
- Law JA, Jacobsen SE. 2010. Establishing, maintaining and modifying DNA methylation patterns in plants and animals. *Nature Reviews. Genetics* 11: 204–220.
- Le T-N, Schumann U, Smith NA, Tiwari S, Khang Au PC, Zhu Q-H, Taylor JM, Kazan K, Llewellyn DJ, Zhang R *et al.* 2014. DNA demethylases target promoter transposable elements to positively regulate stress responsive genes in Arabidopsis. *Genome Biology* 15: 458.
- Lee S, Choi J, Park J, Hong CP, Choi D, Han S, Choi K, Roh TY, Hwang D, Hwang I. 2023. DDM1-mediated gene body DNA methylation is associated with inducible activation of defense-related genes in Arabidopsis. *Genome Biology* 24: 106.
- Lee S, Fu FY, Xu SM, Lee SY, Yun DJ, Mengiste T. 2016. Global regulation of plant immunity by histone lysine methyl transferases. *Plant Cell* 28: 1640–1661.
- Lee TWS, David HS, Engstrom AK, Carpenter BS, Katz DJ. 2019. Repressive H3K9me2 protects lifespan against the transgenerational burden of COMPASS activity in *C. elegans*. *eLife* 8: e48498.
- Li D, Liu RY, Singh D, Yuan XY, Kachroo P, Raina R. 2020. *JMJ14* encoded H3K4 demethylase modulates immune responses by regulating defence gene expression and pipecolic acid levels. *New Phytologist* 225: 2108–2121.
- Li H, Handsaker B, Wysoker A, Fennell T, Ruan J, Homer N, Marth G, Abecasis G, Durbin R, Proc GPD. 2009. The sequence alignment/map format and SAMTOOLS. *Bioinformatics* 25: 2078–2079.
- Li JC, Zhang MQ, Zhou LJ. 2022. Protein S-acyltransferases and acyl protein thioesterases, regulation executors of protein S-acylation in plants. *Frontiers in Plant Science* 13: 956231.
- Li Q, Li HB, Huang W, Xu YC, Zhou Q, Wang SH, Ruan J, Huang SW, Zhang Z. 2019. A chromosome-scale genome assembly of cucumber (*Cucumis sativus* L.). *GigaScience* 8: giz072.
- Li TT, Chen XS, Zhong XC, Zhao Y, Liu XY, Zhou SL, Cheng SF, Zhou DX. 2013. Jumonji C domain protein MJM705-mediated removal of histone H3 lysine 27 trimethylation is involved in defense-related gene activation in rice. *Plant Cell* 25: 4725–4736.
- Lippman Z, Gendrel AV, Black M, Vaughn MW, Dedhia N, McCombie WR, Lavine K, Mittal V, May B, Kasschau KD *et al.* 2004. Role of transposable elements in heterochromatin and epigenetic control. *Nature* 430: 471–476.
- Liu C, Lu F, Cui X, Cao X. 2010. Histone methylation in higher plants. *Annual Review of Plant Biology* 61: 395–420.
- Liu WL, Gallego-Bartolomé J, Zhou YX, Zhong ZH, Wang M, Wongpalee SP, Gardiner J, Feng SH, Kuo PH, Jacobsen SE. 2021. Ectopic targeting of CG DNA methylation in Arabidopsis with the bacterial SssI methyltransferase. *Nature Communications* 12: 3130.
- Liu XC, Luo M, Wu KQ. 2012. Epigenetic interplay of histone modifications and DNA methylation mediated by HDA6. *Plant Signaling & Behavior* 7: 633–635.
- López A, Ramírez V, García-Andrade J, Flors V, Vera P. 2011. The RNA silencing enzyme RNA polymerase V is required for plant immunity. *PLoS Genetics* 7: e1002434.
- Love MI, Huber W, Anders S. 2014. Moderated estimation of fold change and dispersion for RNA-seq data with DESeq2. *Genome Biology* 15: 550.
- Lv DQ, Liu SW, Zhao JH, Zhou BJ, Wang SP, Guo HS, Fang YY. 2016. Replication of a pathogenic non-coding RNA increases DNA methylation in plants associated with a bromodomain-containing viroid-binding protein. *Scientific Reports* 6: 35751.
- Malik HS, Henikoff S. 2003. Phylogenomics of the nucleosome. *Nature Structural Biology* 10: 882–891.
- March-Díaz R, García-Domínguez M, Lozano-Juste J, León J, Florencio FJ, Reyes JC. 2008. Histone H2A.Z and homologues of components of the SWR1 complex are required to control immunity in Arabidopsis. *The Plant Journal* 53: 475–487.
- Marquez-Molins J, Navarro JA, Pallas V, Gomez G. 2019. Highly efficient construction of infectious viroid-derived clones. *Plant Methods* 15: 87.
- Marquez-Molins J, Villalba-Bermell P, Corell-Sierra J, Pallas V, Gomez G. 2023. Integrative time-scale and multi-omics analysis of host responses to viroid infection. *Plant, Cell & Environment* 46: 2909–2927.
- Martínez G, Castellano M, Tortosa M, Pallas V, Gomez G. 2014. A pathogenic non-coding RNA induces changes in dynamic DNA methylation of ribosomal RNA genes in host plants. *Nucleic Acids Research* 42: 1553–1562.
- Martínez G, Pallás V, Gómez G. 2008. Analysis of symptoms developed in plants expressing dimeric forms of Hop stunt viroid. *Journal of Plant Pathology* 90: 121–124.
- Matzke MA, Mosher RA. 2014. RNA-directed DNA methylation: an epigenetic pathway of increasing complexity. *Nature Reviews. Genetics* 15: 394–408.

- Moreno-Romero J, Del Toro-De LG, Yadav VK, Santos-Gonzalez J, Kohler C. 2019. Epigenetic signatures associated with imprinted paternally expressed genes in the Arabidopsis endosperm. *Genome Biology* 20: 41.
- Moreno-Romero J, Jiang H, Santos-Gonzalez J, Kohler C. 2016. Parental epigenetic asymmetry of PRC2-mediated histone modifications in the Arabidopsis endosperm. *EMBO Journal* 35: 1298–1311.
- Mozgova I, Kohler C, Hennig L. 2015. Keeping the gate closed: functions of the polycomb repressive complex PRC2 in development. *The Plant Journal* 83: 121–132.
- Muyle AM, Seymour DK, Lv Y, Huettel B, Gaut BS. 2022. Gene body methylation in plants: mechanisms, functions, and important implications for understanding evolutionary processes. *Genome Biology and Evolution* 14: evac038.
- Navarro B, Flores R, Di Serio F. 2021. Advances in viroid-host interactions. *Annual Review of Virology* 8: 305–325.
- Ng DW, Wang T, Chandrasekharan MB, Aramayo R, Kertbundit S, Hall TC. 2007. Plant SET domain-containing proteins: structure, function and regulation. *Biochimica et Biophysica Acta* 1769: 316–329.
- Palma K, Thorgriksen S, Malinovsky FG, Fiil BK, Nielsen HB, Brodersen P, Hofius D, Petersen M, Mundy J. 2010. Autoimmunity in Arabidopsis is mediated by epigenetic regulation of an immune receptor. *PLoS Pathogens* 6: e1001137.
- Pavet V, Quintero C, Cecchini NM, Rosa AL, Alvarez ME. 2006. Arabidopsis displays centromeric DNA hypomethylation and cytological alterations of heterochromatin upon attack by *Pseudomonas syringae*. *Molecular Plant–Microbe Interactions* 19: 577–587.
- Pecinka A, Dinh HQ, Baubec T, Rosa M, Lettner N, Scheid OM. 2010. Epigenetic regulation of repetitive elements is attenuated by prolonged heat stress in Arabidopsis. *Plant Cell* 22: 3118–3129.
- Pichot C, Djari A, Tran J, Verdenaud M, Marande W, Huneau C, Gautier V, Latrasse D, Arriat S, Somard V *et al.* 2022. Cantaloupe melon genome reveals 3D chromatin features and structural relationship with the ancestral cucurbitaceae karyotype. *Science* 25: 103696.
- Probst AV, Scheid OM. 2015. Stress-induced structural changes in plant chromatin. *Current Opinion in Plant Biology* 27: 8–16.
- Quinlan AR, Hall IM. 2010. BEDTOOLS: a flexible suite of utilities for comparing genomic features. *Bioinformatics* 26: 841–842.
- Raja P, Sanville BC, Buchmann RC, Bisaro DM. 2008. Viral genome methylation as an epigenetic defense against geminiviruses. *Journal of Virology* 82: 8997–9007.
- Ramirez F, Ryan DP, Gruning B, Bhardwaj V, Kilpert F, Richter AS, Heyne S, Dundar F, Manke T. 2016. DEEPTOOLS2: a next generation web server for deep-sequencing data analysis. *Nucleic Acids Research* 44: W160–W165.
- Ramirez-Prado JS, Latrasse D, Rodriguez-Granados NY, Huang Y, Manza-Mianza D, Brik-Chaouche R, Jauannet M, Citerne S, Bendahmane A, Hirt H *et al.* 2019. The Polycomb protein LHP1 regulates stress responses through the repression of the MYC2-dependent branch of immunity. *The Plant Journal* 100: 1118–1131.
- Ramirez-Prado JS, Piquerez SJM, Bendahmane A, Hirt H, Raynaud C, Benhamed M. 2018. Modify the histone to win the battle: chromatin dynamics in plant–pathogen interactions. *Frontiers in Plant Science* 9: 355.
- Roquis D, Robertson M, Yu L, Thieme M, Julkowska M, Bucher E. 2021. Genomic impact of stress-induced transposable element mobility in Arabidopsis. *Nucleic Acids Research* 49: 10431–10447.
- Roudier F, Ahmed I, Berard C, Sarazin A, Mary-Huard T, Cortijo S, Bouyer D, Caillieux E, Duvernois-Berthet E, Al-Shikhley L *et al.* 2011. Integrative epigenomic mapping defines four main chromatin states in Arabidopsis. *EMBO Journal* 30: 1928–1938.
- Rouge M, Quadrana L, Zervudacki J, Hure V, Colot V, Navarro L, Deleris A. 2021. Polycomb mutant partially suppresses DNA hypomethylation-associated phenotypes in Arabidopsis. *Life Science Alliance* 4: e202000848.
- Saha B, Borovskii G, Panda SK. 2016. Alternative oxidase and plant stress tolerance. *Plant Signaling & Behavior* 11: e1256530.
- Schneider CA, Rasband WS, Eliceiri KW. 2012. NIH IMAGE to IMAGEJ: 25 years of image analysis. *Nature Methods* 9: 671–675.
- Schuettengruber B, Martinez AM, Iovino N, Cavalli G. 2011. Trithorax group proteins: switching genes on and keeping them active. *Nature Reviews. Molecular Cell Biology* 12: 799–814.
- Sheikh AH, Nawaz K, Tabassum N, Almeida-Trapp M, Mariappan KG, Alhoraibi H, Rayapuram N, Aranda M, Groth M, Hirt H. 2023. Linker histone H1 modulates defense priming and immunity in plants. *Nucleic Acids Research* 51: 4252–4265.
- Shen QW, Lin YS, Li YB, Wang GF. 2021. Dynamics of H3K27me3 modification on plant adaptation to environmental cues. *Plants-Basel* 10: 1165.
- Singh P, Yekondi S, Chen PW, Tsai CH, Yu CW, Wu KQ, Zimmerli L. 2014. Environmental history modulates pattern-triggered immunity in a HISTONE ACETYLTRANSFERASE1-dependent manner. *Plant Cell* 26: 2676–2688.
- Smotryś JE, Linder ME. 2004. Palmitoylation of intracellular signaling proteins: regulation and function. *Annual Review of Biochemistry* 73: 559–587.
- Snedden WA, Fromm H. 1998. Calmodulin, calmodulin-related proteins and plant responses to the environment. *Trends in Plant Science* 3: 299–304.
- Stassen JHM, López A, Jain R, Pascual-Pardo D, Luna E, Smith LM, Ton J. 2018. The relationship between transgenerational acquired resistance and global DNA methylation in Arabidopsis. *Scientific Reports* 8: 14761.
- Sun J, Zhang Z, Zong X, Huang S, Li Z, Han Y. 2013. A high-resolution cucumber cytogenetic map integrated with the genome assembly. *BMC Genomics* 14: 461.
- Torchetti EM, Pegoraro M, Navarro B, Catoni M, Di Serio F, Noris E. 2016. A nuclear-replicating viroid antagonizes infectivity and accumulation of a geminivirus by upregulating methylation-related genes and inducing hypermethylation of viral DNA. *Scientific Reports* 6: 35101.
- Tran RK, Henikoff JG, Zilberman D, Ditt RF, Jacobsen SE, Henikoff S. 2005. DNA methylation profiling identifies CG methylation clusters in Arabidopsis genes. *Current Biology* 15: 154–159.
- Trejo-Arellano MS, Mehdi S, de Jonge J, Tomastíková ED, Köhler C, Hennig L. 2020. Dark-induced senescence causes localized changes in DNA methylation. *Plant Physiology* 182: 949–961.
- Ueda M, Seki M. 2020. Histone modifications form epigenetic regulatory networks to regulate abiotic stress response. *Plant Physiology* 182: 15–26.
- Wang C, Wang C, Xu W, Zou J, Qiu Y, Kong J, Yang Y, Zhang B, Zhu S. 2018. Epigenetic changes in the regulation of *Nicotiana tabacum* response to cucumber mosaic virus infection and symptom recovery through single-base resolution methylomes. *Viruses* 10: 402.
- Wang HZ, Xiao W, Zhou QB, Chen Y, Yang S, Sheng JS, Yin YQ, Fan J, Zhou JW. 2009. Bystin-like protein is upregulated in hepatocellular carcinoma and required for nucleogenesis in cancer cell proliferation. *Cell Research* 19: 1150–1164.
- Wang Q, Liu P, Jing H, Zhou XF, Zhao B, Li Y, Jin JB. 2021. JMJ27-mediated histone H3K9 demethylation positively regulates drought-stress responses in Arabidopsis. *New Phytologist* 232: 221–236.
- Wang YZ, Hu Q, Wu ZJ, Wang H, Han SM, Jin Y, Zhou J, Zhang ZF, Jiang JF, Shen Y *et al.* 2017. HISTONE DEACETYLASE 6 represses pathogen defence responses in Arabidopsis thaliana. *Plant, Cell & Environment* 40: 2972–2986.
- Wang Z, Baulcombe DC. 2020. Transposon age and non-CG methylation. *Nature Communications* 11: 1221.
- Wibowo A, Becker C, Marconi G, Durr J, Price J, Hagemann J, Papareddy R, Putra H, Kageyama J, Becker J *et al.* 2016. Hyperosmotic stress memory in Arabidopsis is mediated by distinct epigenetically labile sites in the genome and is restricted in the male germline by DNA glycosylase activity. *eLife* 5: e13546.
- Widiez T, Symeonidi A, Luo C, Lam E, Lawton M, Rensing SA. 2014. The chromatin landscape of the moss *Physcomitrella patens* and its dynamics during development and drought stress. *The Plant Journal* 79: 67–81.
- Wu K, Zhang L, Zhou C, Yu CW, Chaikam V. 2008. HDA6 is required for jasmonate response, senescence and flowering in Arabidopsis. *Journal of Experimental Botany* 59: 225–234.
- Wu YL, Lin ZJ, Li CC, Lin X, Shan SK, Guo B, Zheng MH, Li FXZ, Yuan LQ, Li ZH. 2023. Epigenetic regulation in metabolic diseases: mechanisms and advances in clinical study. *Signal Transduction and Targeted Therapy* 8: 98.
- Xu L, Jiang H. 2020. Writing and reading histone H3 lysine 9 methylation in Arabidopsis. *Frontiers in Plant Science* 11: 452.
- Yang TB, Poovaiah BW. 2003. Calcium/calmodulin-mediated signal network in plants. *Trends in Plant Science* 8: 505–512.
- Yelagandula R, Stroud H, Holec S, Zhou K, Feng S, Zhong X, Muthurajan UM, Nie X, Kawashima T, Groth M *et al.* 2014. The histone variant H2A.W



- defines heterochromatin and promotes chromatin condensation in Arabidopsis. *Cell* 158: 98–109.
- Yi H, Riddle NC, Stokes TL, Woo HR, Richards EJ. 2004. Induced and natural epigenetic variation. *Epigenetics* 69: 155–159.
- Yu A, Lepere G, Jay F, Wang J, Bapaume L, Wang Y, Abraham AL, Penterman J, Fischer RL, Voinnet O *et al.* 2013. Dynamics and biological relevance of DNA demethylation in Arabidopsis antibacterial defense. *Proceedings of the National Academy of Sciences, USA* 110: 2389–2394.
- Yu JY, Wu S, Sun HH, Wang X, Tang XM, Guo SG, Zhang ZH, Huang SW, Xu Y, Weng YQ *et al.* 2023. CuGenDBv2: an updated database for cucurbit genomics. *Nucleic Acids Research* 51: D1457–D1464.
- Zeng HQ, Xu LQ, Singh A, Wang HZ, Du LQ, Poovaiah BW. 2015. Involvement of calmodulin and calmodulin-like proteins in plant responses to abiotic stresses. *Frontiers in Plant Science* 6: 600.
- Zeng Z, Zhang W, Marand AP, Zhu B, Buell CR, Jiang J. 2019. Cold stress induces enhanced chromatin accessibility and bivalent histone modifications H3K4me3 and H3K27me3 of active genes in potato. *Genome Biology* 20: 123.
- Zhang X, Clarenz O, Cokus S, Bernatavichute YV, Pellegrini M, Goodrich J, Jacobsen SE. 2007. Whole-genome analysis of histone H3 lysine 27 trimethylation in Arabidopsis. *PLoS Biology* 5: e129.
- Zhao L, Zhou QW, He L, Deng L, Lozano-Duran R, Li GL, Zhu JK. 2022. DNA methylation underpins the epigenomic landscape regulating genome transcription in Arabidopsis. *Genome Biology* 23: 197.
- Zheng J, Chen FY, Wang Z, Cao H, Li XY, Deng X, Soppe WJJ, Li Y, Liu YX. 2012. A novel role for histone methyltransferase KYP/SUVH4 in the control of Arabidopsis primary seed dormancy. *New Phytologist* 193: 605–616.
- Zhou C, Zhang L, Duan J, Miki B, Wu K. 2005. HISTONE DEACETYLASE19 is involved in jasmonic acid and ethylene signaling of pathogen response in Arabidopsis. *Plant Cell* 17: 1196–1204.

## Supporting Information

Additional Supporting Information may be found online in the Supporting Information section at the end of the article.

**Fig. S1** Representative images of mock and HSVd-infected plants.

**Fig. S2** Validation of chromatin immunoprecipitation.

**Fig. S3** Genome browser screenshots of an H3K27me3-enriched gene and an H3K9me2-enriched transposable element.

**Fig. S4** Analysis of the characteristics of H3K9me2- and H3K27me3-enriched regions.

**Fig. S5** Analysis of different characteristics of regions gaining and losing H3K9me2 and H3K27me3.

**Fig. S6** Overlap of H3K9me2 and H3K27me3 gain and loss peaks.

**Fig. S7** Genome browser screenshots of H3K9me2-associated differentially expressed genes.

**Fig. S8** Model for the role of histone modifications during HSVd infection.

**Table S1** Primers used in this study.

**Table S2** Identified H3K9me2 peaks in mock and HSVd-infected plants at 10 and 27 dpi.

**Table S3** Differentially expressed repeats at 10 and 27 dpi.

**Table S4** Identified H3K27me3 peaks in mock and HSVd-infected plants at 10 and 27 dpi.

**Table S5** Genes associated with changes in the different histone marks analyzed.

Please note: Wiley is not responsible for the content or functionality of any Supporting Information supplied by the authors. Any queries (other than missing material) should be directed to the *New Phytologist* Central Office.